THE UNIVERSITY *of* EDINBURGH

The Impact of Intra-Layer Velocity and Density Variations on The Seismic Characterization of a Thin Layer

Amjad AlZawad

THE UNIVERSITY
of EDINBURGH

Thesis submitted in fulfilment of
the requirements for the degree of
Master of Philosophy
to the
University of Edinburgh — 2020

"To my parents, my brother, my sister, my wife Marwa and to everyone who supported me and made this accomplishment possible"

Abstract

Seismic exploration has progressed greatly in the past 75 years due to advances in seismic acquisition and processing. One interpretation technique used by geoscientists is measuring amplitude-variations-with-offset (AVO). AVO analysis helps in understanding elastic property changes, lithology identification, rock properties and pore fluid properties to assist in gas and oil exploration. Interpretations of AVO responses could be complicated by the presence of thin layers which cause tuning. Tuning occurs when the thickness between two layers is very small to the extent that it would be hard to distinguish the boundaries between two interfaces.

The main focus of my thesis is to investigate the effect of varying velocity and density within a thin layer on seismic characterization using tuning curves and AVO analysis.

For my study, I chose the Primary Pulse Method. This method considers gradual changes in velocity and density between two welded elastic half spaces but ignores the effect of multiples. I coded the equations of the Primary Pulse Method then compared my results with the published results and got good similarities.

I extended the work of the published method to investigate the impact of varying velocity and density on waveform shapes. The results showed that the intra-layer velocity and density changes do have an impact on waveform shapes for the top and bottom of a transition zone model. My investigation of tuning curves

indicated that the Primary Pulse Method results diverge as thickness tends to zero. I hypothesized that this effect could be a result of ignoring multiples in the Primary Pulse Method and confirmed this by comparing it with the Reflectivity Method.

To asses the practical implications of these results, I analyzed seismic responses from a well log data set. The Primary Pulse Method still gave unrealistic high amplitudes which confirms the importance of ignoring multiples. On the other hand, one of the advantages of the Primary Pulse Method is considering the effect of ray bending which my results showed it could have a potential impact on AVO analysis.

I concluded that varying velocities and densities can have implications on thin layer characterization but I recommend that the Primary Pulse Method should not be used to study thin layers.

Lay Summary

Imagine rays of sunlight shining through a window into a room. Now imagine a mirror intercepting these rays, this will cause the rays of light to reflect off the mirror in a certain direction. These rays can be considered as seismic waves, which have a certain speed (velocity) and a certain strength (amplitude), and the mirror as a layer in the Earth's subsurface. When a seismic wave passes through the Earth's subsurface, it gets reflected back to the surface and recorded by special equipments called geophones. This recorded data is then analysed to get a better understanding of the Earth's subsurface geology and structure. The time it takes the wave to reach a layer then reflects back to the surface is called the two-way travel time. Each layer in the subsurface can be considered as a mirror, so every time a wave reaches a layer it gets reflected back to the surface. When a wave reflects off a layer that has a very small thickness (thin layer) and gets recorded, the seismic data would show only one reflection leading to incorrect interpretations (i.e. tuning). Tuning occurs when the thickness between two layers is insignificant it becomes hard to distinguish between them. Thin layers and the tuning effect are the main focus of my thesis. To analyze the effect of thin layers and tuning, I used an equation that calculates the seismic responses of thin subsurface layers and I compared it with similar published equations.

The primary seismic response method i used in this thesis is called the Primary Pulse Method. This method assumes a gradual increase in velocity and density

as the wave moves through the subsurface. I compared The Primary Pulse Method with the Acoustic Impedance equation which assumes a sudden increase in velocity and density. Acoustic Impedance calculates the contrast between two layers based on the wave velocity and density reflected off the layers. When I examined the results, I found that the travel time of both methods is the same but the Primary Pulse Method showed unreasonably high amplitude responses.

Next, I sought to investigate amplitude variations with offset (AVO). Offset is the distance between the source of a seismic wave and the geophone that records the reflected wave and it depends on the angle the seismic wave reflects off a layer in the subsurface. I compared the effects of AVO on the Primary Pulse Method and on the Shuey equation. Shuey's equation is similar to Acoustic Impedance as both equations assume a sudden increase in wave velocity and density. However, Shuey's equation considers the angle the wave reflects off a layer. Comparing the AVO responses of both methods showed unreasonably high amplitudes for the Primary Pulse Method but similar waveform responses at angles less than 10° with more pronounced differences as the angle increases from 10° to 30°.

An important concept to consider in seismic analysis is multiples. When a wave reflects off a layer, it might not reach the surface immediately. Instead, it might reflect between the layers in the subsurface before finally reaching the surface. This effect results in multiples which would appear as a reflection response in seismic data but in reality it is a misleading response. The Primary Pulse Method does not consider the effect of multiples which I believe is the reason for the unrealistic high amplitude responses.

To verify the effect of multiples, I compared the Primary Pulse Method with the Reflectivity method which considers multiples. The results I got showed that ignoring multiples in the Primary Pulse Method does indeed cause unrealistic high amplitudes.

Finally, I decided to compare the effect of ray bending on seismic responses for AVO analysis. Ray bending is the change of the wave's angle as it moves through the subsurface due to changes in velocity and density. I compared the responses of the Shuey equation with and without ray bending. The results showed that ray bending does produce different AVO analysis.

I concluded from my investigation that the Primary Pulse Method should not be used on thin layers cases. Moreover, applying the Shuey equation with ray bending showed potential to be considered for AVO analysis.

Acknowledgements

I would like to express my deep gratitude and thanks to my supervisor Dr. Mark Chapman for all of his support, time and guidance. I would also like to thank Prof. Anton Ziolkowski and Dr.Georgios Papageorgiou whose expertise were invaluable in the completion of this thesis.

I would like to thank Saudi Aramco for their unending support to sponsor me for this MPhil program.

Finally, I wish to thank my friends specially Ali Shaiban, my family and my wife Marwa AlHawaj for their continuous encouragement and help to get me through these past years of study. This accomplishment would not have been possible without them. Thank you.

Contents

List of Figures

Introduction

Thin layers have always been a subject of interest in seismic exploration due to their abundant presence in the subsurface and the complications that arise in seismic interpretations as a result of tuning. Tuning occurs when a layer thickness is small to the point it is hard to distinguish between layer boundaries. Tuning will result in strong constructive or destructive seismic responses that represents the geology of the subsurface in a more complex way. The presence of thin layers will result in abnormal Amplitude Variations with Offset (AVO) responses.

AVO is the study of amplitude variations with offset for a given seismic reflection due to changes in the reflection coefficient with incident angle. This technique is used in seismic interpretation due to its valuable contribution in the detection of hydrocarbons, reservoir characterization and prospect evaluation. AVO is based on the work of Knott (1899) and Zoeppritz (1919) but their equations were too complex to implement in seismic analysis. A number of authors (Bortfeld (1961), Aki and Richards (1980), Shuey (1985)) approximated simpler angle dependent reflection coefficients by linearizing the complex Knott (1899) and Zoeppritz (1919) equations. One of the prominent equations used in the industry today is the Shuey equation which assumes abrupt velocity and density changes for an interface between two elastic media (block model). However, in reality the interface should be represented as a complex velocity and density model.

This thesis focuses on the impact of applying a method that takes into account gradual variations in velocity and density on thin layer characterization and evaluating its results by comparing them with current AVO methods that assume sudden changes in velocity and density. My method of choice is the Primary Pulse Method. This method considers gradual changes in velocity and density between two welded elastic half spaces but ignores the effect of multiples.

In this thesis, I start by providing an introduction and background information to seismic exploration, AVO Analysis, the Primary Pulse Method, thin layers and tuning. Then, I illustrate the coding of the Primary Pulse Method equations, I validate my results with the published results and I compare my results with the reflection coefficient equation of Acoustic Impedance. Afterwards, I evaluate the results of the Primary Pulse Method when applied on thin layer cases and compare my results with the Shuey equation, which ignores multiples, and the Reflectivity Method, which considers the effect of multiples. My applications and comparisons are performed on modeled data examples and well log data sets.

Chapter 1

Background

1.1 A Brief History of Seismic Exploration and AVO Analysis

In 1921 a group of scientists conducted a historical experiment using dynamite and a seismograph to record the responses of seismic waves traveling in the subsurface of the Earth. The recording showed reflections resulting from a boundary between two seismic layers. This experiment was initiated to check the possibility of using seismic data in gas and oil exploration. The results from this experiment were just the beginning of seismic exploration. Throughout the past 75 years, seismic exploration has advanced remarkably. These days different methods (e.g. vibrator, dynamite and air gun) are used as seismic sources, acquisition is done on land and sea, seismic receivers (geophones) are smaller and lighter in weight and seismic surveys are designed as an array of geophones to get a better signal to noise ratio (Dragoset (2005), Hesthammer *et al.* (2001), Milligan (2004), Yilmaz (2001), Ongkiehong and Askin (1988)). By studying and interpreting seismic data, geoscientists can evaluate fluid content, rock lithology

and can, to some degree, predict the possibility of a hydrocarbon prospect in a defined area (Selley and Sonnenberg (2014), Telford *et al.* (1976), Sheriff (1976), Barclay *et al.* (2008), Gao (2003), Granli *et al.* (1999)). To help them with their interpretation, scientists use a couple of important parameters: Reflection amplitudes (strength of the reflection) , layer thickness, reflector continuity, wave velocity, wave frequency and wave phase (Mondol (2010), Yilmaz (2001)). Geoscientists would also use quantitative techniques for the detection of hydrocarbons, reservoir characterization and prospect evaluation. The most important of those techniques are measuring Amplitude-Variations-with-Offset (AVO), amplitude analysis (bright spots), forward modeling and seismic inversion. I will focus on AVO analysis because of its great impact on hydrocarbon detection in the seismic industry (Aki and Richards (1980), Sheriff and Geldart (1995), Ville (1948), James (2003), James (2009)).

AVO analysis and interpretation is the study of amplitude variations at an interface between two elastic media due to changes in the reflection coefficient (how much energy is reflected/transmitted) as a function of offset (Zhang and Brown (2001), Blangy (1994), Carcione and Tinivella (2000)) (Figure 1.1). AVO is used in the industry today because of its valuable contributions to understand elastic property changes, lithology identification, hydrocarbon detection, rock properties and pore fluid properties (Garotta and Grange (1987), Loizou *et al.* (2008), Xie (2005), Zhang and Brown (2001) ,Chiburis (1984)). Its fundamentals are based on an incident plane wave, Snell's law (1.1), the assumption of a singular isotropic boundary between two elastic half spaces; with continuous displacements and stresses across that boundary (Figure 1.2) and sharp changes in amplitude between the two elastic half spaces (Zhang and Brown (2001), Castagna and Backus (1993)).

Snell's law

$$s = \frac{\sin\theta_1}{\alpha_1} = \frac{\sin\theta_2}{\alpha_2} = \frac{\sin\phi_1}{\beta_1} = \frac{\sin\phi_2}{\beta_2}, \tag{1.1}$$

where:

s = ray parameter

α_1 = P-wave velocity in medium 1 α_2 = P-wave velocity in medium 2

β_1 = SV-wave velocity in medium 1 β_2 = SV-wave velocity in medium 2

θ_1 = P-wave angle of incidence θ_2 = P-wave angle of transmission

ϕ_1 = SV-wave angle of reflection ϕ_2 = SV-wave angle of transmission

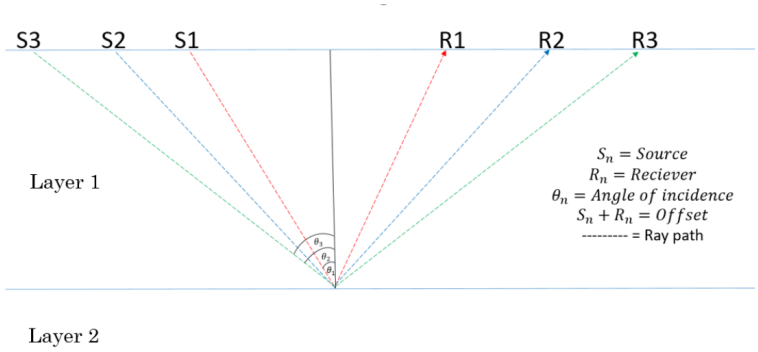

Figure 1.1. Simple representation of AVO components that show how source and receiver positions affect the angle of incidence.

Early work of Knott (1899) and Zoeppritz (1919) are the basis of AVO analysis and interpretation but their equations were too complex to fully understand and implement in seismic data. Bortfeld (1961), Richards and Frasier (1976), Aki and Richards (1980) and Shuey (1985) produced simpler approximations for the angle-dependent P-wave reflection coefficient R(θ) by linearizing the Knott (1899) and Zoeppritz (1919) equations. Bortfeld (1961) approximated the reflection coefficient by implementing Snell's law and the general equations of discrete changes with the assumptions of an incident plane wave with angles smaller than 30°, an isotropic single layer transition boundary between two welded elastic

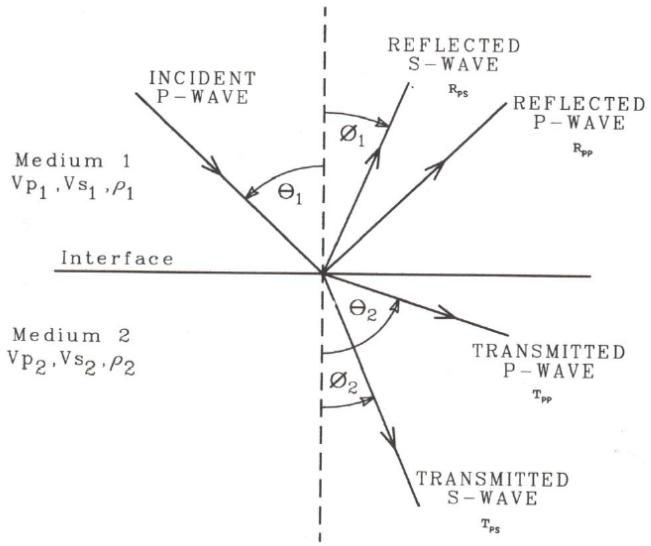

Figure 1.2. Reflection and transmission components of an incident P-wave upon a boundary between two elastic half-spaces as noted by Snell's law (Figure taken from Castagna and Backus (1993)).

media (continuous displacements and stresses across the boundary) and small changes in elastic parameters (1.2).

$$R(\theta) = \frac{1}{2}[\frac{\Delta\alpha}{\alpha}\frac{1}{cos^2\theta_1} + \frac{\Delta\rho}{\rho} - 4\sin^2\phi_1(2\frac{\Delta\beta}{\beta} + \frac{\Delta\rho}{\rho})], \tag{1.2}$$

where:

θ_1= P-wave angle of incidence, θ_2= P-wave angle of transmission

ϕ_1= SV-wave angle of reflection, ϕ_2= SV-wave angle of transmission

$\alpha = \frac{\alpha_1+\alpha_2}{2}$, $\Delta\alpha = \alpha_2 - \alpha_1$

$\beta = \frac{\beta_1+\beta_2}{2}$, $\Delta\beta = \beta_2 - \beta_1$

ρ_1= density of medium 1, ρ_2= density of medium 2, $\rho = \frac{\rho_1+\rho_2}{2}$, $\Delta\rho = \rho_2 - \rho_1$

1.2 AVO Analysis Today

A simpler form of equation 1.2 that includes approximations for the reflection coefficient intercept (A) and slope (B) for small changes in elastic parameters was given by Shuey (1985) (1.3), with similar assumptions as Bortfeld (1961).

$$R(\theta) = A + B\sin^2(\theta), \tag{1.3}$$

where: $A = \frac{\Delta\alpha}{2\alpha} + \frac{\Delta\rho}{2\rho}$, $B = \frac{\Delta\alpha}{2\alpha} - 4\frac{\beta^2}{\alpha^2}(\frac{\Delta\rho}{2\rho} + \frac{\Delta\beta}{\beta})$, and θ= angle of incidence

This equation was the starting point of using AVO analysis in hydrocarbon detection. By cross-plotting the reflection coefficient intercept (A) and slope or gradient (B), AVO responses can be interpreted and used in the detection of gas sands (Fatti *et al.* (1994), Kelly and Ford (2000a),Kelly and Ford (2000b), Smith and Gidlow (1987)). Castagna *et al.* (1998) shows that in the A-B plane brine-saturated sandstones and shales follow a well-defined background trend based on petrophysical assumptions. Deviations from this background can indicate hydrocarbons or abnormal lithological elastic properties (AVO anomalies) (Castagna and Backus (1993), Castagna *et al.* (1985), Goodway *et al.* (1997), Gray *et al.* (1999)). From these deviations Rutherford and Williams (1989) defined three unique classes for gas-sand AVO anomalies (class I, class II and class III) by comparing the acoustic impedance contrast of the gas sands with the surrounding shale. Class I shows higher impedance contrast than the surrounding shale , class II shows similar impedance contrast to the surrounding shale and class III shows lower impedance contrast than the surrounding shale. Then Castagna and

Swan (1997) built on Rutherford and Williams (1989) work and suggested a more accurate interpretation, where instead of a hydrocarbon sand classification based on R(θ) alone it should also be on their position in the A-B plane (quadrant I,II,III and IV) (Figure 1.3). This new classification subdivided class III gas sands to class III and IV where although both classes show lower impedance contrast than the surrounding shale, the reflection coefficient decreases with increasing offset for class IV (Figures 1.3 and 1.4) (Castagna *et al.* (1998), Cambois (1998), Foster *et al.* (1997)).

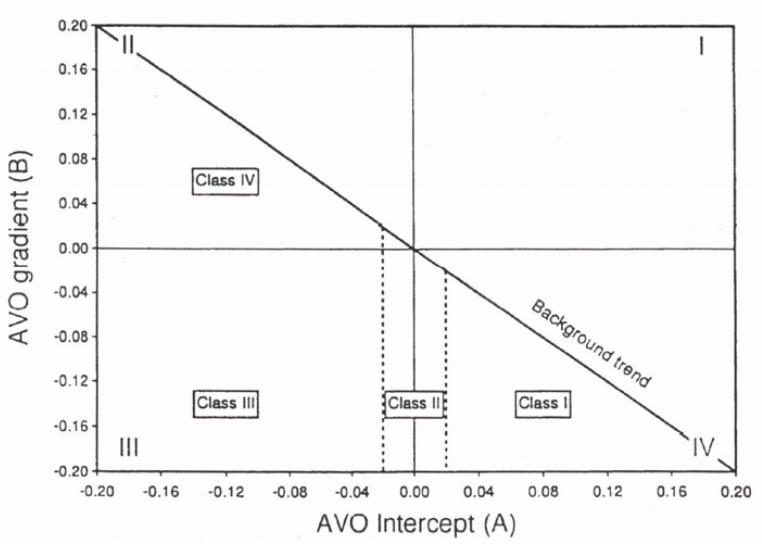

Figure 1.3. Class I sands have a high-impedance contrast while Class II sands have similar-impedance contrast. Class III sands have low-impedance contrast but is subdivided into Class III and IV based on Castagna *et al.* (1998) (Numbers in the corners are quadrant numbers) (Figure taken from Castagna *et al.* (1998)).

Class	Relative Impedance	Quadrant	A	B	Amplitude vs. Offset
I	Higher than overlying unit	IV	+	-	Decreases
II	About the same as the overlying unit	II, III, or IV	+ or -	-	Increase or decrease; may change sign
III	Lower than overlying unit	III	-	-	Increases
IV	Lower than overlying unit	II	-	+	Decreases

Figure 1.4. This table shows the AVO response of each class of the Castagna and Swan (1997) gas sand classification (Figure taken from Castagna and Swan (1997)).

Another concept to help interpret AVO anomalies is called the fluid line. From equation 1.3, Foster and Keys (1999) derived an expression for the intercept A and slope B for AVO responses resulting from changes in rock properties (1.4).

$$B = (1 - 8\gamma^2)A; \tag{1.4}$$

this equation is called the fluid line, where: A is the intercept, B is the slope and $\gamma = \frac{\beta}{\alpha}$.

Applying this concept in the slope-intercept domain (Figure 1.5) demonstrates that wet sand and shale reflections fall on or near the fluid line, while gas or hydrocarbon bearing sand reflections fall on a trend parallel and on opposite sides of the fluid line. The deviation from the fluid line is highest with gas, lowest with brine while oil-sands lie in the region between. Since rock properties of sands and shale differ, sand/shale interface reflections trends are displaced from the fluid line with a distance depending on $\frac{1}{\gamma}$. Additionally, porosity changes move the AVO response along trends approximately parallel to the fluid line because although they affect acoustic impedance, they do not significantly impact $\frac{1}{\gamma}$ (Dong (1996)). Using all of these observations can be valuable in the interpretation of

AVO anomalies, as shown in Figure 1.5. It is important to note that any AVO anomaly should be interpreted within the context of an appropriate geological model (Castagna *et al.* (1998), Foster *et al.* (2010), Hilterman (1989), Hilterman (1990)).

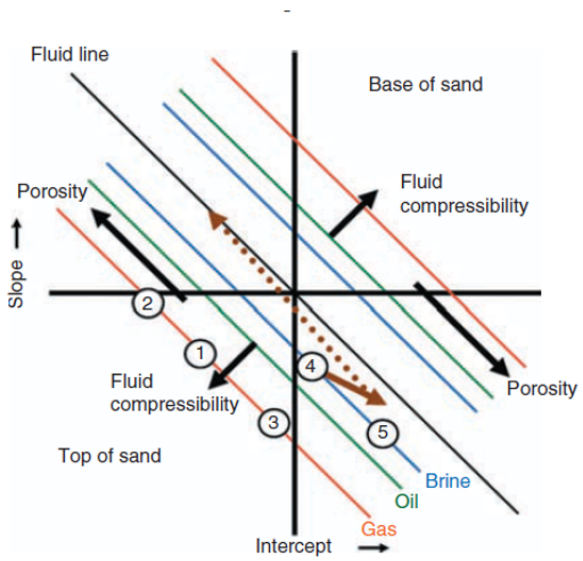

Figure 1.5. The effect of reservoir properties changes on the top of sand AVO response. 1: class III gas sand response; 2: higher-porosity gas sand response; 3: lower-porosity gas sand response; 4: wet-sand response (by replacing gas with brine); 5: lower porosity wet-sand response. The solid brown arrow shows the effect of adding clay to the pore space in a shaly sand and the dashed brown arrow shows the effect of adding clay beyond the critical concentration (Figure taken from Foster *et al.* (2010)).

1.3 The Primary Pulse Method

Bortfeld (1961)'s reflection coefficient approximations and assumptions for AVO were defined with the assumption that the reflected and transmitted waves are of known pulse shapes and have sharp amplitude changes at layer boundaries.

However, Richards and Frasier (1976) addressed the issue of what would be the primary scattered pulse shapes that result from an incident plane wave of a known pulse shape upon a depth dependent inhomogeneity (transition zone) between two elastic media (Figures 1.6 and 1.7). These figures show all possible ray paths the incident P and SV waves might take.

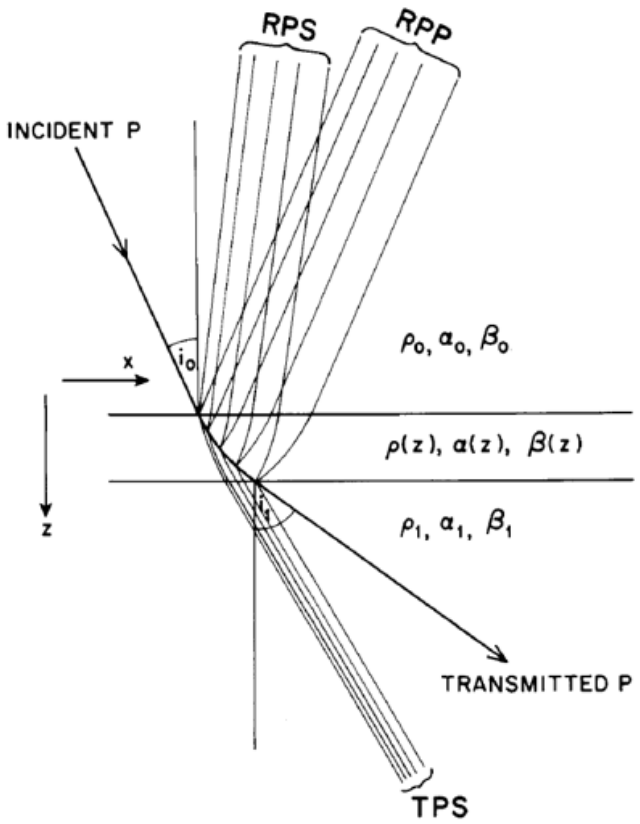

Figure 1.6. Primary scattered waves resulting from an incident plane P-wave on a transition zone (Figure taken from Richards and Frasier (1976)).

where $_0$ denotes parameters of the upper half space and $_1$ denotes parameters of the lower half space.

Figures 1.6 and 1.7 show a three letter naming convention used for the primary pulse shapes (RPP, RPS, TPS, RSP, RSS and TSP). Where the first letter is used as R for reflection or T for transmission, the second letter is the incident

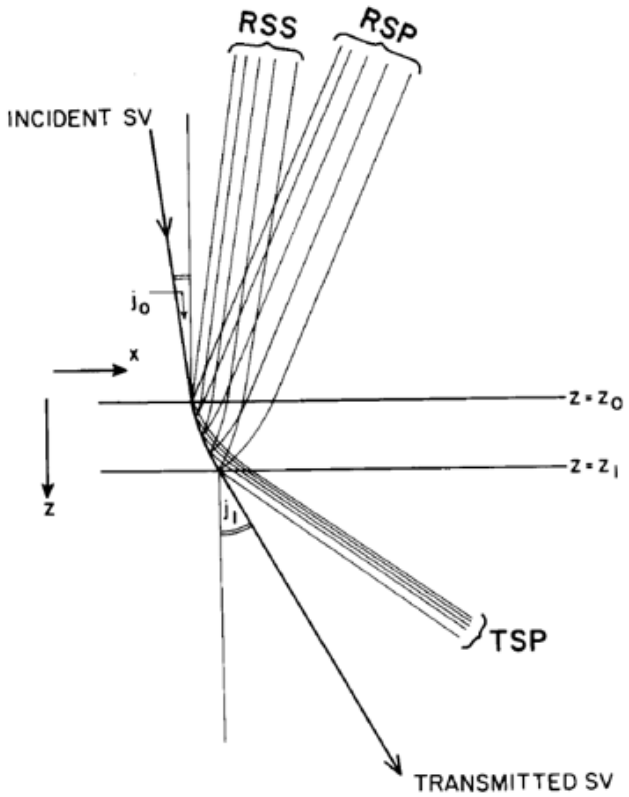

Figure 1.7. Primary scattered waves resulting from an incident plane SV-wave (vertical plane propagation) on a transition zone (Figure taken from Richards and Frasier (1976)).

wave type, P-wave or SV-wave and the final letter is the type of wave reflected, transmitted or converted which could be a P or SV wave.

Through the assumption of a single isotropic layer interface with small changes of density and velocity, between two welded homogeneous half spaces, they expressed the reflected compressional incident wave amplitude as:

$$\Delta rpp = (\cos 2\phi - \frac{1}{2})\frac{\Delta\rho}{\rho} + \frac{1}{2\cos^2\theta}\frac{\Delta\alpha}{\alpha} - 4\sin^2\phi\frac{\Delta\beta}{\beta}; \tag{1.5}$$

which is just another form of Bortfeld (1961)'s equation (1.2).

To implement their method, Richards and Frasier (1976) modeled the transition zone as a sequence of thin homogeneous layers and assumed no multiples in their calculations. They used geometrical ray theory as a basis, then took the incident wave as an impulse of known shape and calculated the amplitude using equation 1.5. They calculated the particle velocity at any depth through the transition zone and took the sum of the reflected P-waves at each thin layer in the transition zone as the thickness approaches zero. From their calculations, they got an equation for the P-wave reflection coefficient RPP(ω) (1.6).

$$RPP(\omega) = \int_{z_0}^{z_1} \lim_{\Delta\zeta\to 0} \frac{\Delta rpp}{\Delta\zeta} \exp\left[-\theta\omega[sx + 2\tau_\alpha(z_0,\zeta)]\right] d\zeta, \tag{1.6}$$

where:

z_0= top of transition, z_1= bottom of transition, ζ= depth, $\Delta\zeta$ = change in depth , s= slowness = ray parameter in equation 1.1 , ω= frequency , x= displacement, $\tau_\alpha(z_0,\zeta) = \int_{z_0}^{\zeta} \frac{\cos\theta(z)}{\alpha(z)} dz$.

Finally, by changing the integration variable from depth (ζ) to time ($t = t(\zeta) = sx + 2\tau_\alpha(z,\zeta)$, the top and bottom of the transition zone can be used as the limits of the integrand in the time domain; but since the integrand is zero outside the transition zone it can be calculated for $-\infty < t < \infty$. By applying similar calculations for each primary pulse shape, Richards and Frasier (1976) developed 6 primary pulse shape solutions in the time domain (The Primary Pulse Method) (Equations 1.7 - 1.28). Although there are two more reflection coefficient equations (TPP and TSS), they are not utilized in this method because they are not considered primary reflection equations. These two equations are calculated from at least two interactions in the transition zone which result in multiples, while the Primary Pulse Method ignores the effect of multiples.

Incident P-Wave Pulse Shape Equations:

Incident P-wave with reflected P-wave:

$$RPP(t) = \frac{d(rpp)}{d\zeta} \cdot \frac{\alpha(\zeta)}{2\cos\theta(\zeta)}, \tag{1.7}$$

where:

$$t = sx + 2\tau_\alpha(z_0,\zeta), \tag{1.8}$$

$$\tau_\alpha(z_0,\zeta) = \int_{z_0}^{\zeta} \frac{\cos\theta(z)}{\alpha(z)} dz \tag{1.9}$$

$$\frac{d(rpp)}{d\zeta} = (\frac{1}{2} - 2s^2\beta^2)\frac{\rho'}{\rho} + \frac{1}{2(1-s^2\alpha^2)}\frac{\alpha'}{\alpha} - 4s^2\beta^2\frac{\beta'}{\beta}. \tag{1.10}$$

Incident P-wave with reflected SV-wave:

$$RPS(t) = \frac{d(rps)}{d\zeta} \cdot \frac{1}{\frac{\cos\theta}{\alpha} + \frac{\cos\phi}{\beta}} \cdot \frac{A_\alpha(z_0,\zeta)}{A_\beta(z_0,\zeta)}, \tag{1.11}$$

where:

$$t = sx + \tau_\alpha(z_0,\zeta) + \tau_\beta(z_0,\zeta), \tag{1.12}$$

$$\frac{d(rps)}{d\zeta} = s\alpha[\sqrt[2]{1-s^2\alpha^2}\frac{\beta}{\alpha} + \frac{1-2s^2\beta^2}{2\sqrt[2]{1-s^2\beta^2}}]\frac{\rho'}{\rho} + 2s\beta[\sqrt[2]{1-s^2\alpha^2} - \frac{s^2\alpha\beta}{\sqrt[2]{1-s^2\beta^2}}]\frac{\beta'}{\beta}, \tag{1.13}$$

$$\tau_\beta(z_0,\zeta) = \int_{z_0}^{\zeta} \frac{\cos\phi(z)}{\beta(z)} dz, \tag{1.14}$$

$$A_\alpha(z_0,\zeta) = \sqrt[2]{\frac{\rho_0\alpha_0\cos\theta_0}{\rho(\zeta)\alpha(\zeta)\cos\theta(\zeta)}}, \tag{1.15}$$

$$A_\beta(z_0,\zeta) = \sqrt[2]{\frac{\rho_0\beta_0\cos\phi_0}{\rho(\zeta)\beta(\zeta)\cos\phi(\zeta)}}, \tag{1.16}$$

Incident P-wave with transmitted SV-wave:

$$TPS(t) = \frac{d(tps)}{d\zeta} \cdot \frac{1}{\frac{\cos\phi}{\beta} - \frac{\cos\theta}{\alpha}} \cdot \frac{A_\alpha(z_0,\zeta)}{A_\beta(z_1,\zeta)}, \tag{1.17}$$

where:

$$t = sx + \int_{z_0}^{\zeta} \frac{\cos\theta(z)}{\alpha(z)} dz + \int_{\zeta}^{z_1} \frac{\cos\phi(z)}{\beta(z)} dz \tag{1.18}$$

$$\frac{d(tps)}{d\zeta} = s\alpha[\sqrt[2]{1-s^2\alpha^2}\frac{\beta}{\alpha} - \frac{1-2s^2\beta^2}{2\sqrt[2]{1-s^2\beta^2}}]\frac{\rho'}{\rho} + 2s\beta[\sqrt[2]{1-s^2\alpha^2} + \frac{s^2\alpha\beta}{\sqrt[2]{1-s^2\beta^2}}]\frac{\beta'}{\beta}. \tag{1.19}$$

Incident SV-Wave Pulse Shape Equations:

Incident SV-wave with reflected P-wave:

$$RSP(t) = \frac{d(rsp)}{d\zeta} \cdot \frac{1}{\frac{\cos\theta}{\alpha} + \frac{\cos\phi}{\beta}} \cdot \frac{A_\beta(z_0,\zeta)}{A_\alpha(z_0,\zeta)} \tag{1.20}$$

where:

$$t = sx + \tau_\alpha(z_0,\zeta) + \tau_\beta(z_0,\zeta) \tag{1.21}$$

$$\frac{d(rsp)}{d\zeta} = \frac{\beta\sqrt[2]{1-s^2\beta^2}}{\alpha\sqrt[2]{1-s^2\alpha^2}} \frac{d(rps)}{d\zeta} \tag{1.22}$$

Incident SV-wave with reflected SV-wave:

$$RSS(t) = \frac{d(rss)}{d\zeta} \cdot \frac{\beta(\zeta)}{2\cos\phi(\zeta)} \tag{1.23}$$

where:

$$t = sx + 2\tau_\beta(z_0,\zeta) \tag{1.24}$$

$$\frac{d(rss)}{d\zeta} = (2s^2\beta^2 - \frac{1}{2})\frac{\rho'}{\rho} + [4s^2\beta^2 - \frac{1}{2(1-s^2\beta^2)}]\frac{\beta'}{\beta} \tag{1.25}$$

Incident SV-wave with transmitted P-wave:

$$TSP(t) = \frac{d(tsp)}{d\zeta} \cdot \frac{1}{\frac{\cos\phi}{\beta} - \frac{\cos\theta}{\alpha}} \cdot \frac{A_\beta(z_0,\zeta)}{A_\alpha(z_1,\zeta)} \tag{1.26}$$

where:

$$t = sx + \int_{z_0}^{\zeta} \frac{\cos\phi(z)}{\beta(z)}dz + \int_{\zeta}^{z_1} \frac{\cos\theta(z)}{\alpha(z)}dz \tag{1.27}$$

$$\frac{d(tsp)}{d\zeta} = \frac{-\beta\sqrt[2]{1-s^2\beta^2}}{\alpha\sqrt[2]{1-s^2\alpha^2}}\frac{d(tps)}{d\zeta} \tag{1.28}$$

1.4 Richards and Frasier Results

To evaluate the accuracy of the Primary Pulse Method, Richards and Frasier (1976) compared it first with the Haskell (1953) Matrix Method. This method, which is an extension of the Thomson (1950) Matrix Method, computes the reflection coefficient in the frequency domain to model the frequency dependent effect of a layer and it considers the effect of multiples (Chapman (2003)). The Primary Pulse Method and Haskell (1953)'s Method are applied for the cases of incident plane waves upon a transition zone such that the sum of travel times at each thin layer equals the total travel time through the transition zone which preserves time. The comparison showed good correlation for the reflected waves with minor differences when using a velocity gradient or a density

gradient separately but it presented more pronounced differences in the case of using a density and velocity gradient together. As for the transmitted waves, the comparison indicated excellent correlation for all incident angles between 0° and 30°.

Next, to assess the Primary Pulse Method viability in the presence of high order scattering, Frasier (1970)'s discrete time method is used for comparison. This method accumulates the multiple-reflected pulses directly in time by a matrix multiplication. Results show decent agreement between both methods with more pronounced differences at critical angles due to high order scattering. Finally, to compare the accuracy of the Primary Pulse Method in the frequency domain, Richards and Frasier (1976) applied the Papoulis (1962) Polygon Method on the Primary Pulse Method to convert it to the frequency domain then compared the result to Haskell (1953)'s Method; which is naturally in the frequency domain. Results show that the Primary Pulse Method is accurate at frequencies greater than 0.3 Hz and shows minor inaccuracies at lower frequencies. However, the method fails drastically with low frequencies at critical angles of incidence and would create problems in the presence of a turning point in the medium. Although the Primary Pulse Method is inadequate at low frequencies, since it ignores low frequency multiples and uses geometrical ray theory for incident wave transmission, shortcomings are not usually seen on recorded data because of the low-frequency cut-off in seismic recording systems (Richards and Frasier (1976)). The results of Richards and Frasier (1976) indicates the potential of applying the Primary Pulse Method as a mathematically simple method on AVO analysis by taking into consideration gradual changes in velocity, density and changes in angle of incidence due to ray bending. This method can be applied as an alternative to current reflection coefficient equations that assume sudden changes in velocity and density with a constant angle of incidence through a transition zone (e.g. Shuey (1985)'s equation).

1.5 Thin Layers and The Tuning Effect

Thin layers have always been a subject of interest in seismology; especially for reservoir hydrocarbon detection because of their abnormal AVO response which is a result of seismic amplitude tuning (Bakke and Ursin (1998), Ball (1988), Swan (1988)). Tuning, or simply layer interference, results in a strong constructive or destructive seismic response that might represent more complex geology. Tuning is affected by the thickness or spacing between the top and bottom boundaries of a chosen seismic interface (e.g. transition zone) and by the dominant period of the incident wave (Bakke and Ursin (1998), Hindlet and McDonald (1986), Ursin and Dahl (1992)). It was proven by Widess (1973) that reflection amplitude changes with layer thickness. Widess (1973) also defined tuning thickness as the thickness equal to one quarter of the dominant wavelength in the signal.

1.6 The Sleipner Vest Gas Field

To resolve issues and short comings of thin layers, a number of authors provided different suggestions and methods to calculate to some degree thickness, velocity, frequency and amplitude of a thin layer (spectral decomposition, spectral inversion and full waveform inversion) (Chadwick *et al.* (2010), Furre *et al.* (2017), Romdhane *et al.* (2014), Velis and Rubino (2011), Williams and Chadwick (2012)). These methods were used on the Sleipner Vest gas field which was discovered in 1974. In 1996, Statoil and partners injected CO_2 separated from natural gas in the porous and saline Utsira Formation in the Sleipner field. This was done in response to the Norwegian CO_2 emissions tax to avoid pollution and to meet gas sale requirements (Furre *et al.* (2017)). CO_2 was injected at a yearly rate of around 0.9 Mt from 1996 to this day. The CO_2 containment in the Utsira Formation was monitored throughout the years using seismic and gravimeter data

(Alnes *et al.* (2008), Arts *et al.* (2008), Boait *et al.* (2012), Furre *et al.* (2017)). The monitoring has confirmed containment of the CO_2 in the Utsira Formation and has provided significant data to be used in thin layer detection methods.

1.7 Thin Layer Detection Methods

Since thin layers are imaged as tuned wavelets (two wavelets that appear as one due to tuning), then spectral decomposition can be used to predict their temporal (travel time) thickness. Spectral decomposition or simply time-frequency analysis decomposes the data into its frequency and phase components which helps in thin layer imaging resolution and temporal thickness (Farfour *et al.* (2017)). Williams and Chadwick (2012) used the Wigner-Ville Distribution (WVD) and the Smoothed Pseudo Wigner-Ville Distribution (SPWVD) as their spectral decomposition method (Ville (1948), Wigner (1997)). Figures 1.8 and 1.9 show results for different spectral decomposition algorithms that have been applied on a synthetic trace with different frequencies. In Figure 1.9, the SPWVD shows good spectral information in detecting individual CO_2 layers. Although the method was used on 2D data, it can also be used on 3D data. From these results, it can be observed that the temporal thickness of the top most layer in the plume is in agreement with the rock physics since all the necessary parameters of the top seal to use the SPWVD efficiently were already known. However, the method does not work as well when used deeper in the plume since the layers are too closely spaced together and can not be easily distinguished. These results could possibly be used to derive true layer velocities (Williams and Chadwick (2012), Ursin (1990), Ursin and Ekren (1995), Chung and Lawton (1995)).

Another thin layer detection method is spectral inversion. Inversion is the opposite of forward modeling, it uses measured data and applies a specified

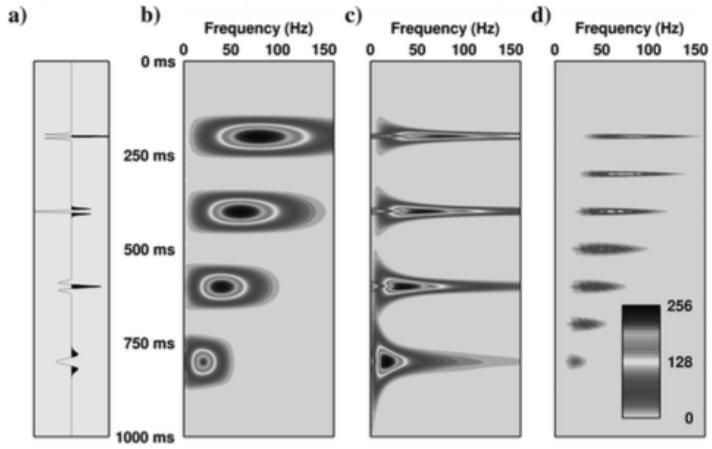

Figure 1.8. (a) A synthetic trace of Ricker wavelets (zero-phase wavelets) with a sampling rate of 1 ms and peak frequencies of 80, 60, 40, and 20 Hz. Frequency decomposition using (b) the windowed Fourier transform (128-point Hanning window), (c) the continuous wavelet transform, and (d) the WVD method (Figure taken from Williams and Chadwick (2012))

.

operation or mathematical equation that inverts the data back to an Earth model. The result should be a model that is relatively similar to the Earth's subsurface (Barclay *et al.* (2008), Huang and Zhang (2013), Castaño and Ojeda (2010), Castaño *et al.* (2011)). Spectral inversion, inverts measured frequency and phase data to get an Earth model. Velis and Rubino (2011) show that spectral inversion can provide information in determining CO_2 saturated thin layer thicknesses and compressional velocities in the Sleipner Vest gas field. By comparing compressional velocity values with CO_2 saturation, they observed that compressional velocity is mostly sensitive to low CO_2 saturation (Figure 1.10). For layer thickness and velocity experiments, Velis and Rubino (2011) kept all parameters constant except for velocity and density which had specified wide search ranges (Figure 1.11) and used near offset seismic stack gathers for inversion (Figure 1.12). To analyze and compare the results, they chose three different thicknesses (3m, 6.5m and 10m), two CO_2 saturation's (0.0 and 0.1) and two

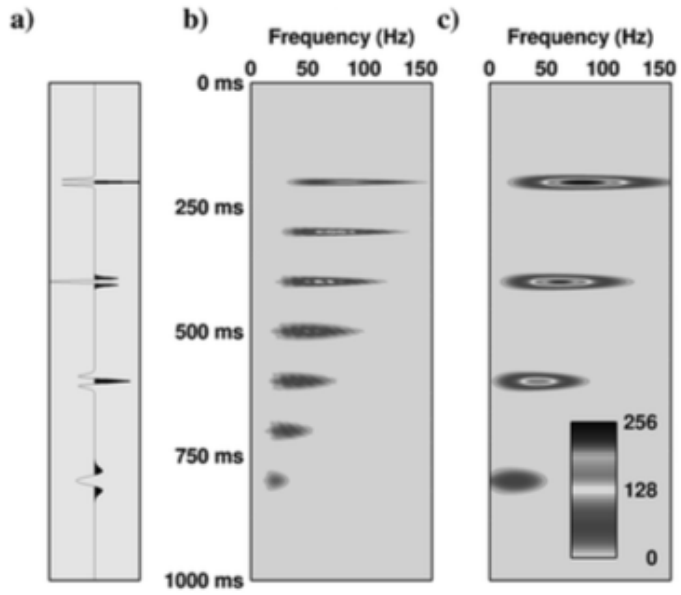

Figure 1.9. (a) A synthetic trace of Ricker wavelets (zero-phase wavelets) with a sampling rate of 1 ms and peak frequencies of 80, 60, 40, and 20 Hz. Frequency decomposition using (b) the WVD method and (c) the SPWVD method (Figure taken from Williams and Chadwick (2012)).

signal to noise ratios (50 and 10). Examining Figure 1.13 and Figure 1.14, it can be observed that the results are in good agreement but with a bigger uncertainty in compressional velocity than in layer thickness (Velis and Rubino (2011)).

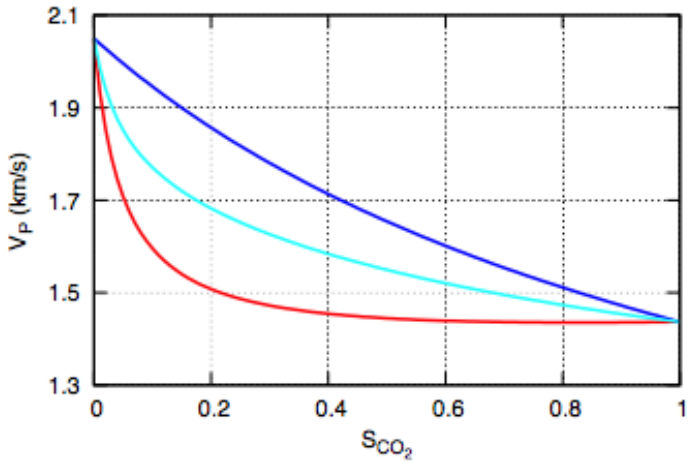

Figure 1.10. The effect of frequency and Co2 saturation on compressional velocity. Low frequency compressional velocities (red), high frequency compressional velocities (blue) and average compressional velocity (cyan) as functions of CO_2 saturation (Figure taken from Velis and Rubino (2011)).

Lithology	V_P (km/s)	V_S (km/s)	ρ (gr/cm^3)
Nordland Fm.	2.15–2.38	0.80–0.89	1.99–2.20
Utsira Sand ($S_{CO_2} = 0.95$)	1.37–1.51	0.63–0.70	1.85–2.05
Utsira Sand (diffuse CO_2)	1.3–2.3	0.61–0.68	1.96–2.16

Figure 1.11. Spectral inversion parameter and thin-bed thickness ranges (Figure taken from Velis and Rubino (2011)).

One more method to detect thin layers is Full Waveform Inversion (FWI). This method calculates the differences between a modeled and observed seismic waveform to obtain a high resolution velocity model. (Romdhane *et al.* (2014), Kamei and Lumley (2015), Schmid *et al.* (2016), Ratcliffe *et al.* (2011)). Romdhane *et al.*

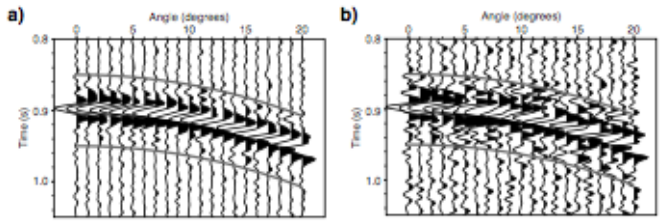

Figure 1.12. Example of a seismic gather used to generate near-offset spectral inversion stacks. (a) S/N = 50 and (b) S/N = 10 with Vp=1.77 km/s, a thickness of 3m and CO_2 concentration of 0.1 (Figure taken from Velis and Rubino (2011)).

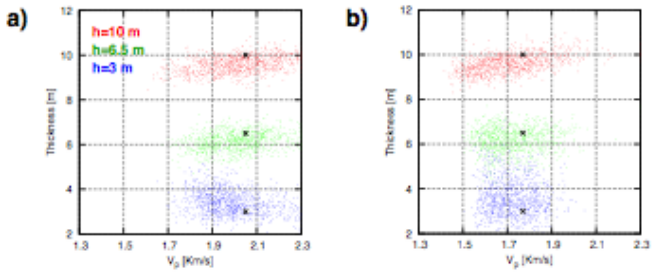

Figure 1.13. Spectral inversion results after 1000 iterations (S/N = 50) (a) CO_2 concentration of 0.0, (b) CO_2 concentration of 0.1 (small black x represents the true value) (Figure taken from Velis and Rubino (2011)).

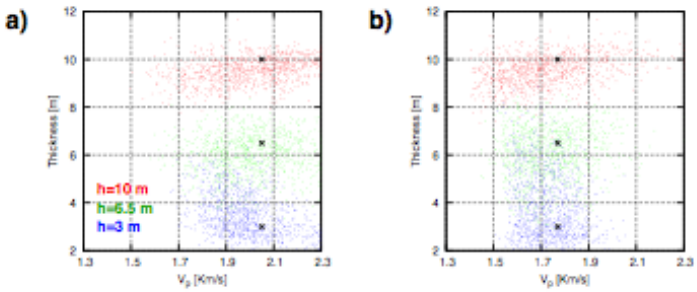

Figure 1.14. Spectral inversion results after 1000 iterations (S/N = 10) (a) CO_2 concentration of 0.0, (b) CO_2 concentration of 0.1 (small black x represents the true value) (Figure taken from Velis and Rubino (2011)).

(2014) showed the effect of using FWI on synthetic and real data. They showed that applying FWI on synthetic data improved the resolution of the initial velocity model and had better identification of the velocities and thicknesses of the thin CO_2 layers. For real data, the Sleipner 2008 data was used. First, some pre-proessing was done to improve the signal to noise ratio. Then, by applying FWI for frequencies up to almost 40Hz they were able to identify the geometry of the thin CO_2 layers in the plume and the lateral extend of the CO_2 plume.

Chapter 2

METHODOLOGY

2.1 Coding The Primary Pulse Method

The first step of conducting my tests was to reproduce the results of the Primary Pulse Method to compare them with Richards and Frasier (1976) results. I used python for my coding and I chose the RPP equation which is an incident plane P-wave reflected as a P-wave (1.7) as an example to demonstrate the coding process. I chose the RPP equation since most seismic interpretation and analysis is done on primary waves.

I applied the RPP equation on one of Richards and Frasier (1976) three-layer models (Figure 2.1). Each three-layer model is represented as a 5 km transition zone sandwiched between two homogeneous half spaces. The transition zone is approximated by a sequence of thin layers with equal thickness based on a 0.05 second two-way travel time of the SV waves. This results in 67 layers for model 1 and 53 layers for models 2 and 3. For my example, I applied the RPP equation on model 3 which has both a velocity and density gradient. Since the 5 km transition

zone in model 3 is divided into 53 thin layers with equal thicknesses, each thin layer thickness is approximated as 0.09 km.

Table 2. Parameters of upper and lower half-spaces for each model. Between the half-spaces is a 5-km thick transition zone in which parameters vary linearly between their half-space values.

	Model 1	Model 2	Model 3
Upper Half-Space			
ρ_0	2.0 gm/cc	3.0	2.0
α_0	5.0 km/sec	5.0	5.0
β_0	3.0	3.0	3.0
Transition Zone, 5 km thick			
Lower Half-Space			
ρ_1	3.5	3.0	3.5
α_1	5.0	8.0	8.0
β_1	3.0	4.8	4.8

Figure 2.1. Richards and Frasier's three-layer model parameters (Figure taken from Richards and Frasier (1976)).

I then estimated the elastic parameter derivatives (ρ', α', β') using Taylor series (2.1) (Abramowitz and Stegun (1965)).

$$f(x+h) \approx f(x)+hf'(x)+h^2\frac{f''(x)}{2} \quad , \quad f(x-h) \approx f(x)-hf'(x)+h^2\frac{f''(x)}{2} \quad (2.1)$$

where:

$f(x)$ = the elastic parameter of a chosen layer (ρ, α or β)

$f'(x)$ = the elastic parameter derivative of a chosen layer (ρ', α' or β')

h = the thickness of a chosen layer in the transition zone

$f(x+h)$ = the elastic parameter of the layer above my chosen layer

$f(x-h)$ = the elastic parameter of the layer below my chosen layer

To get a better approximation and reduce the error of the Taylor series in 2.1, I utilized the equation of the form:

$$f'(x) \approx \frac{f(x+h) - f(x-h)}{2h} \tag{2.2}$$

I used a time function defined from 0 to 6 seconds with the first reflection arrival time at 1 sec for all incident angles. Then, to calculate the two-way arrival time, I used the RPP time series (2.3) with x=1; since the displacement is defined as one unit step in the direction of propagation.

$$t = sx + 2\tau_\alpha(z_0, \zeta) \tag{2.3}$$

where:

s is the slowness and $\tau_\alpha(z_0, \zeta) = \int_{z_0}^{\zeta} \frac{\cos\theta(z)}{\alpha(z)} dz$.

To calculate the ray parameter or slowness "s", which is constant throughout the transition zone, I implemented Snell's law on the initial P-wave angle of incidence and initial P-wave velocity. Then, from the velocity gradient, Snell's law and slowness I calculated the angle of incidence at each thin layer as the wave moves throughout the transition zone (2.4).

$$\theta = \arcsin(s * \alpha) \tag{2.4}$$

The next step was to approximate the integration term of the time series equation $\tau_\alpha(z_0, \zeta)$. The method I decided to use was the Trapezoidal Rule.

The Trapezoidal Rule is a method of integration that calculates a definite integral by approximating the area under the graph of the integrated function as a number of trapezoids. I chose the Trapezoidal Rule (2.5) due to its simplicity and reliability as a definite integration technique (Atkinson (2008)).

$$\int_a^b f(x) = \frac{\Delta x}{2}(f(x_0) + 2(f(x_1) + f(x_2) + f(x_3) + ...) + f(x_n)) \tag{2.5}$$

where: $\Delta x = \frac{b-a}{n}$ and n is the number of iterations.

To evaluate the sufficient number of iterations needed for the Trapezoidal Rule, I plotted an integral convergence graph based on the number of iterations (Figure 2.2).

I noticed from the plot that the integral converges quickly at 10 iterations and stays constant beyond that number. This means I can use 50 iterations for the Trapezoidal Rule without compromising the results of the integral. Although 50 iterations were enough for this example, I also plotted integral convergence graphs for all the Primary Pulse Method equations for every model and confirmed that 50 iterations is more than enough for all results.

Finally, to compare my results with Richards and Frasier (1976), I used the same

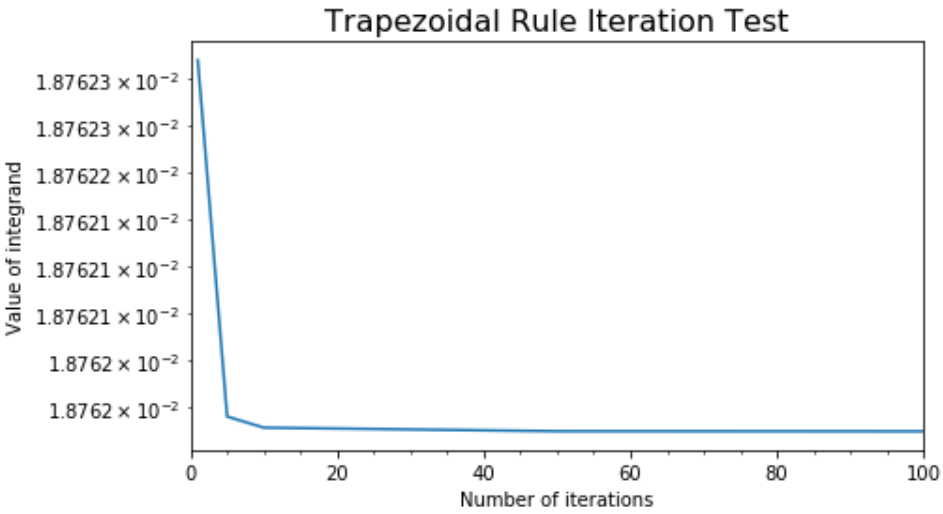

Figure 2.2. The graph shows the result of applying the Trapezoidal Rule on the definite integral using different numbers of iterations. The integral converges quickly around 10 iterations.

4 initial angles of incidence they used on model 3 for the RPP equation (0°, 10°, 20° and 30°). In my results, each angle of incidence is represented by a different color:

θ_i=0 is in Red, θ_i=10 is in Blue, θ_i=20 is in Green, and θ_i=30 is in Cyan.

After running my codes, I got the plot on the right hand side in Figure 2.5.

2.2 Richards and Frasier's Results

Figures 2.3 to 2.20 compare my coded results with Richards and Frasier (1976) results for the layer models defined in figure 2.1:

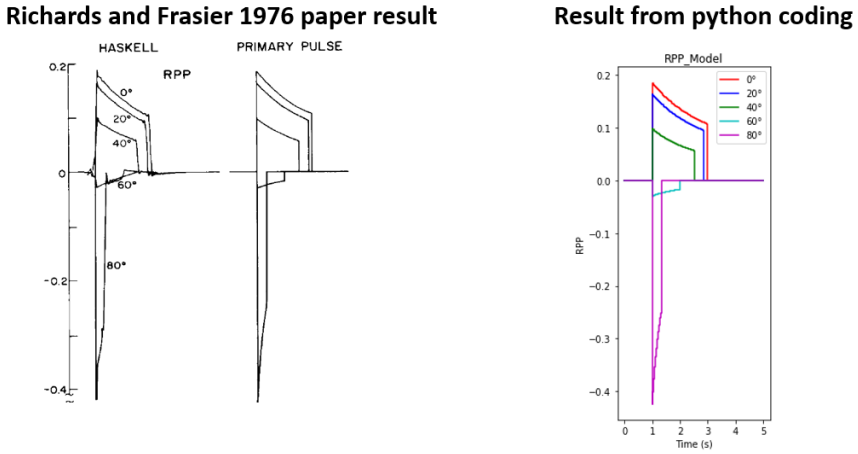

Figure 2.3. RPP python code result for model 1. On the left is Richards and Frasier (1976) results and on the right is my coded result.

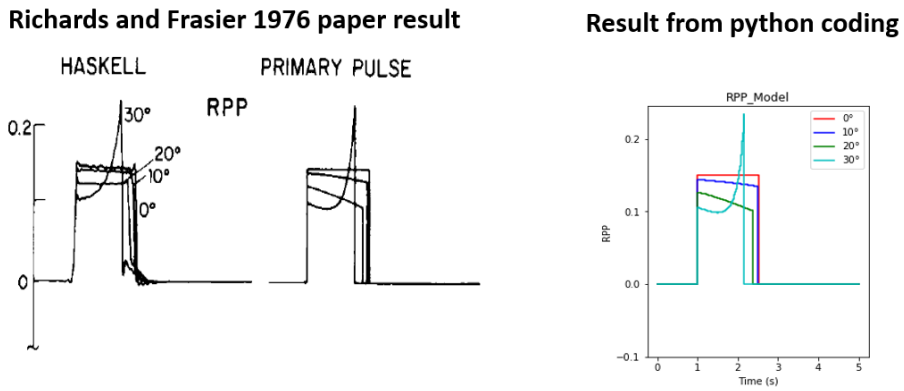

Figure 2.4. RPP python code result for model 2. On the left is Richards and Frasier (1976) result and on the right is my coded result.

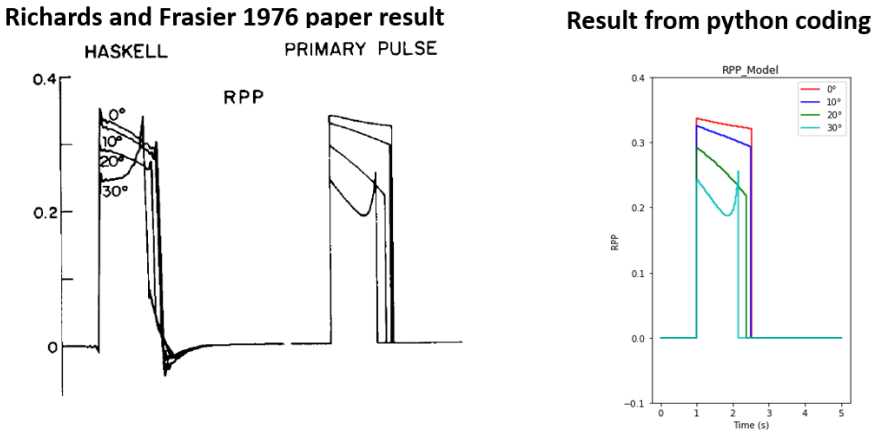

Figure 2.5. RPP python code result for model 3. On the left is Richards and Frasier (1976) result and on the right is my coded result.

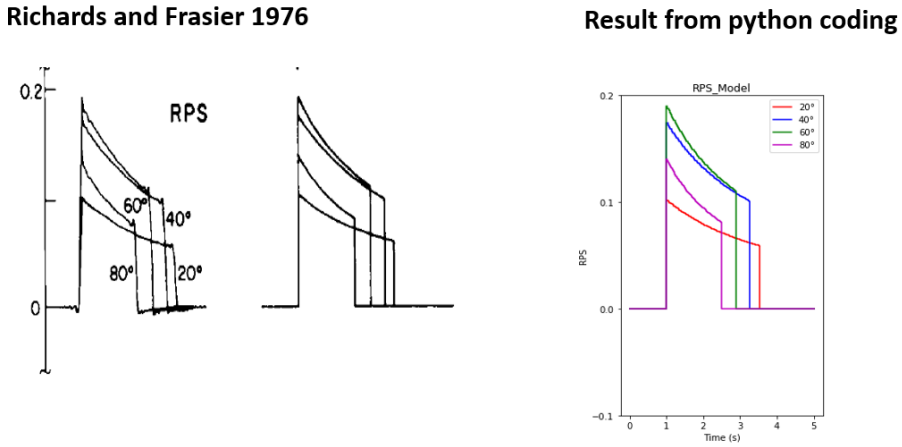

Figure 2.6. RPS python code result for model 1. On the left is Richards and Frasier (1976) result and on the right is my coded result.

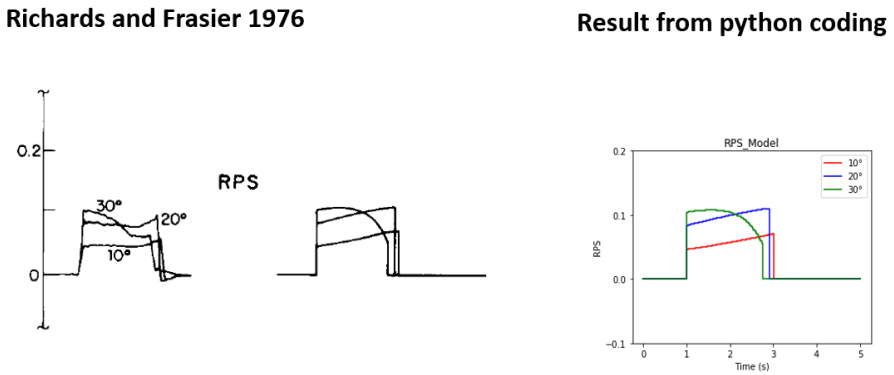

Figure 2.7. RPS python code result for model 2. On the left is Richards and Frasier (1976) result and on the right is my coded result.

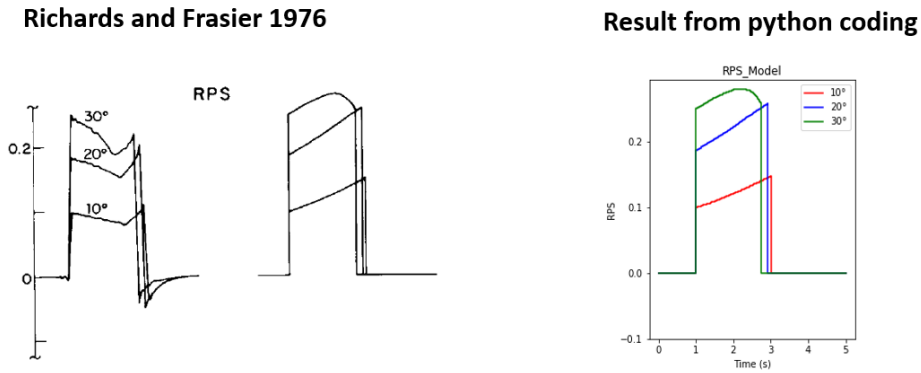

Figure 2.8. RPS python code result for model 3. On the left is Richards and Frasier (1976) result and on the right is my coded result.

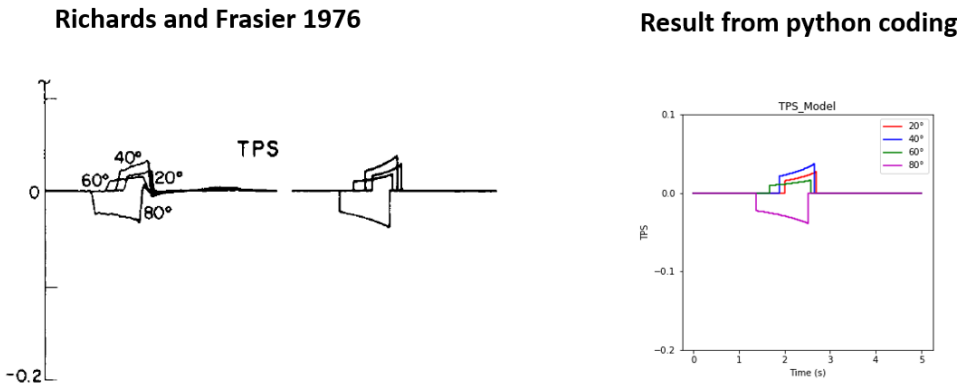

Figure 2.9. TPS python code result for model 1. On the left is Richards and Frasier (1976) result and on the right is my coded result.

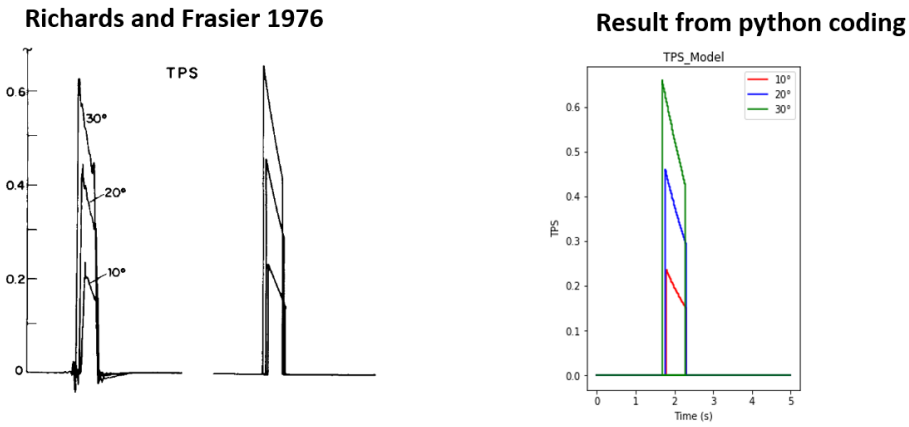

Figure 2.10. TPS python code result for model 2. On the left is Richards and Frasier (1976) result and on the right is my coded result.

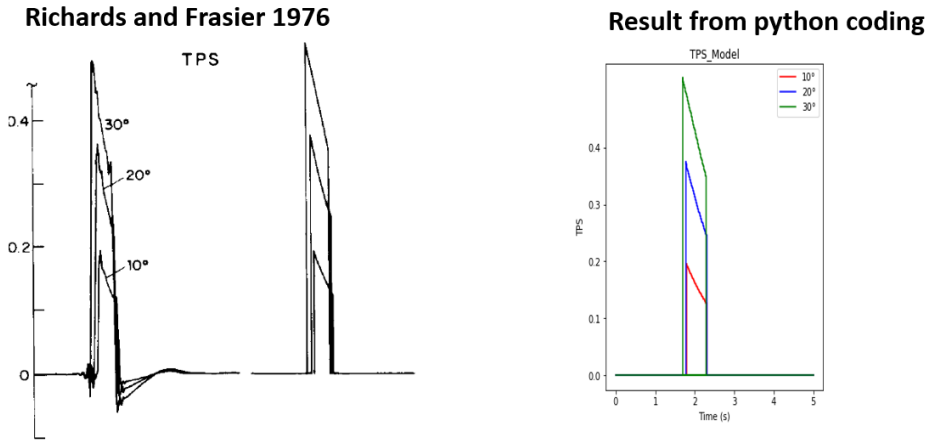

Figure 2.11. TPS python code result for model 3. On the left is Richards and Frasier (1976) result and on the right is my coded result.

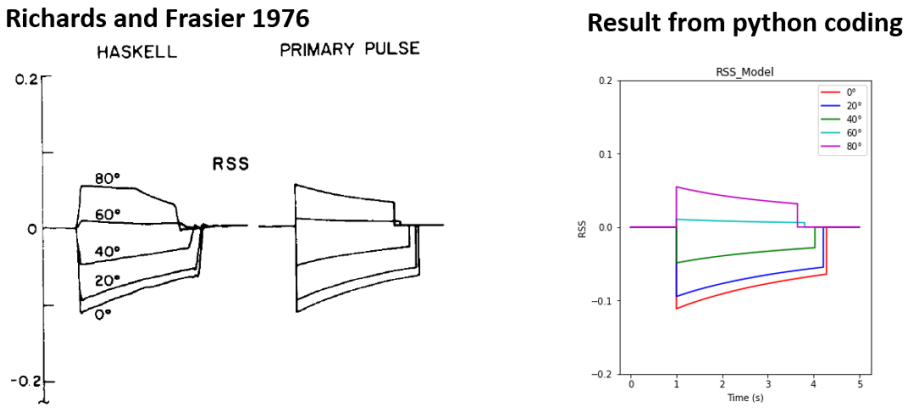

Figure 2.12. RSS python code result for model 1. On the left is Richards and Frasier (1976) result and on the right is my coded result.

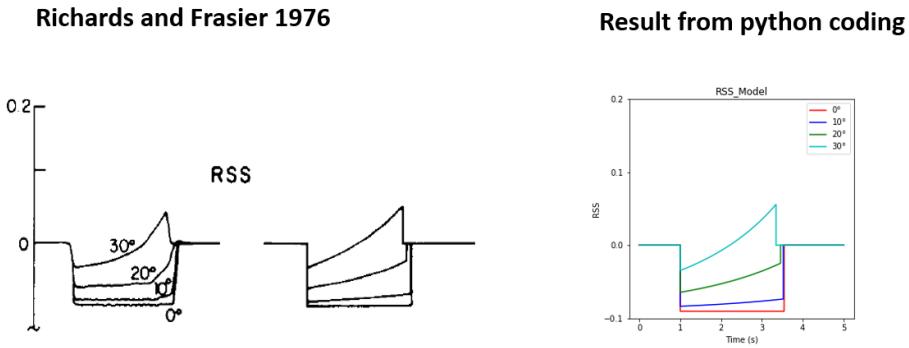

Figure 2.13. RSS python code result for model 2. On the left is Richards and Frasier (1976) result and on the right is my coded result.

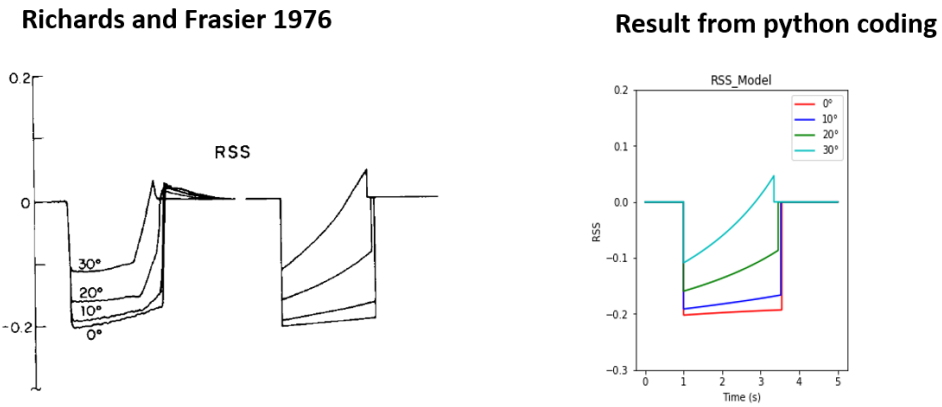

Figure 2.14. RSS python code result for model 3. On the left is Richards and Frasier (1976) result and on the right is my coded result.

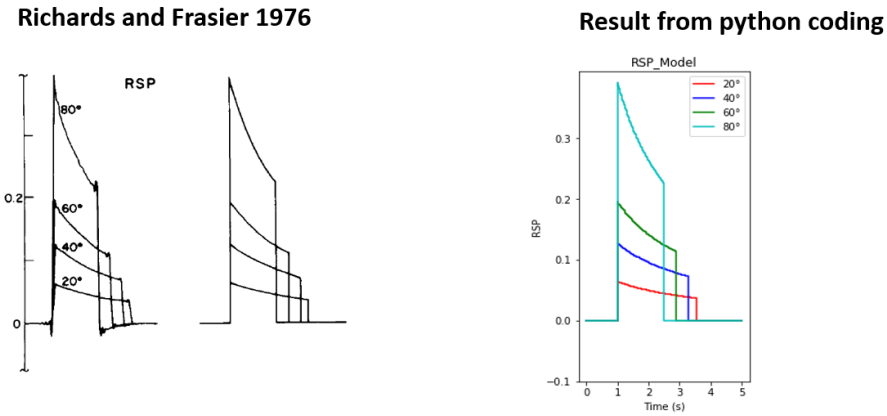

Figure 2.15. RSP python code result for model 1. On the left is Richards and Frasier (1976) result and on the right is my coded result.

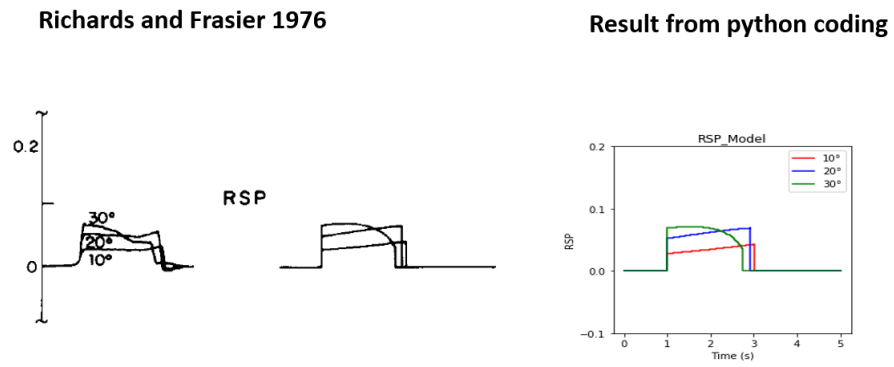

Figure 2.16. RSP python code result for model 2. On the left is Richards and Frasier (1976) result and on the right is my coded result.

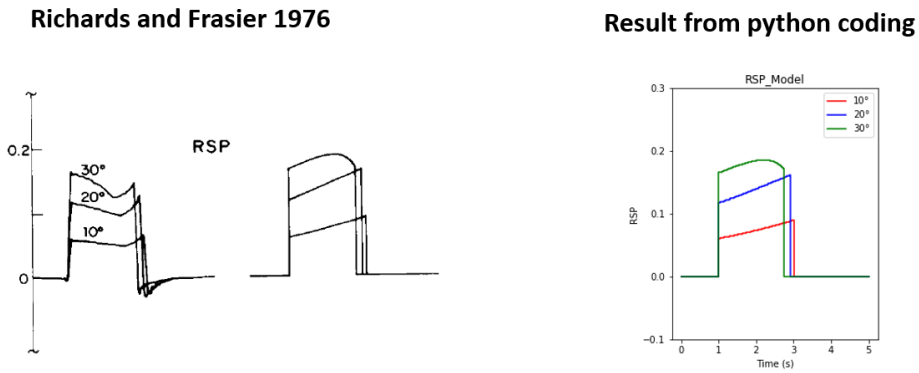

Figure 2.17. RSP python code result for model 3. On the left is Richards and Frasier (1976) result and on the right is my coded result.

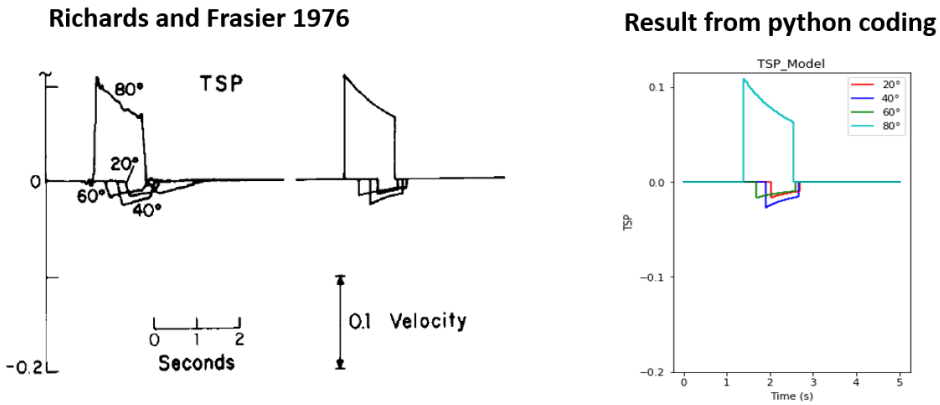

Figure 2.18. TSP python code result for model 1. On the left is Richards and Frasier (1976) result and on the right is my coded result.

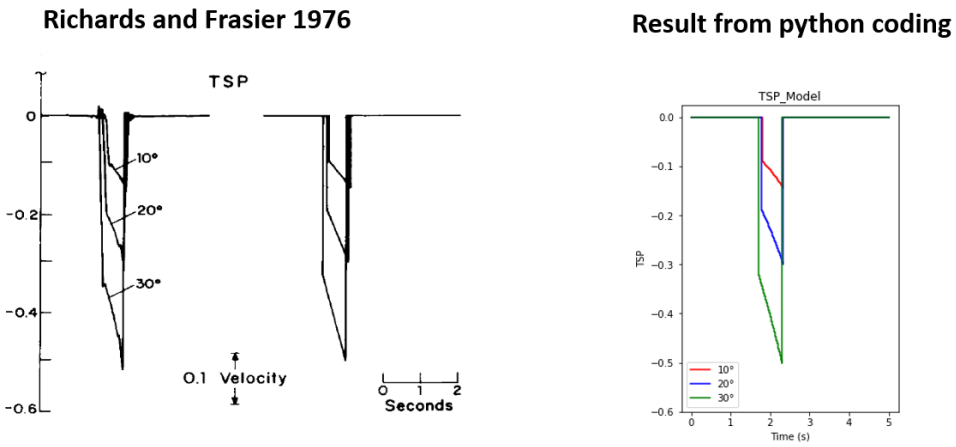

Figure 2.19. TSP python code result for model 2. On the left is Richards and Frasier (1976) result and on the right is my coded result.

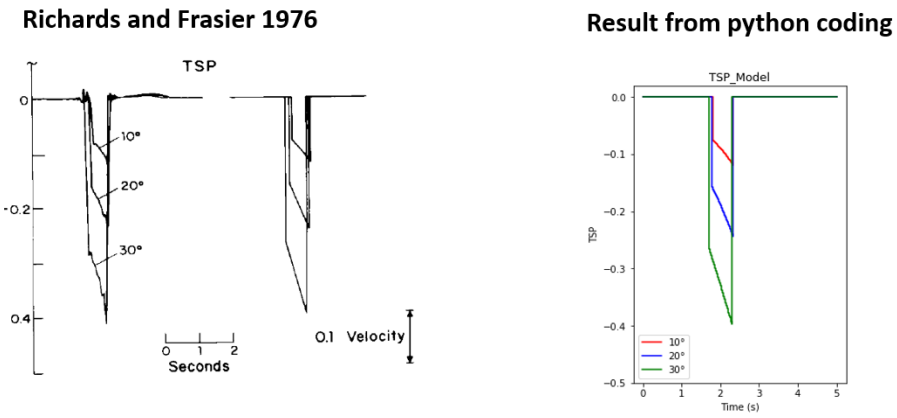

Figure 2.20. TSP python code result for model 3. On the left is Richards and Frasier (1976) result and on the right is my coded result.

Examining all the previous figures shows good agreement between my results and Richards and Frasier (1976) results.

2.3 The Application of The Primary Pulse Method on Vertical Propagation

To evaluate the seismic waveforms of the Primary Pulse Method, I convolved the RPP equation responses with a 30 Hz Ricker wavelet (Figure 2.21). For my example, I convolved the RPP result of model 3 at vertical incidence (θ_i=0 degrees) (Figure 2.22) with the Ricker wavelet .

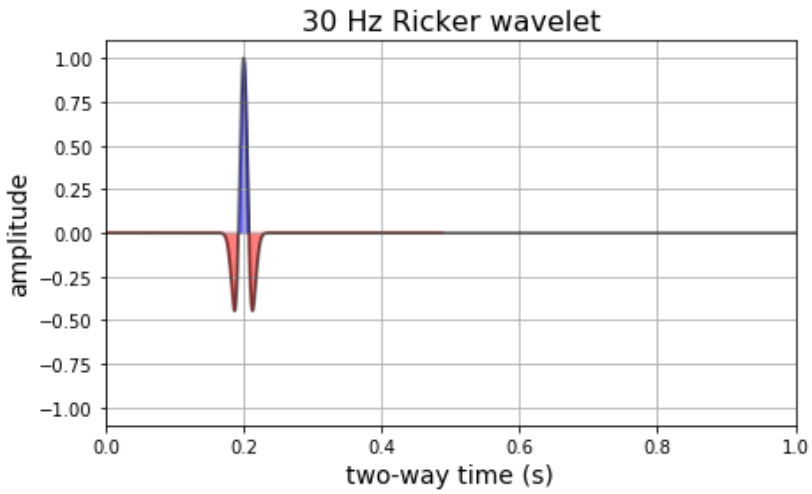

Figure 2.21. 30 Hz Ricker wavelet at 0.2s central time, max amplitude of 1, 6001 samples and 0.001s sampling rate.

Before applying the convolution, both the RPP result and Ricker wavelet must have the same number of samples and sampling rate. I chose a sufficient number of samples for my convolution; if it was small then the wavelet would not resolve and if it was large then it would unnecessarily increase computing time with no significant impact on the results. To get the same number of samples and sampling

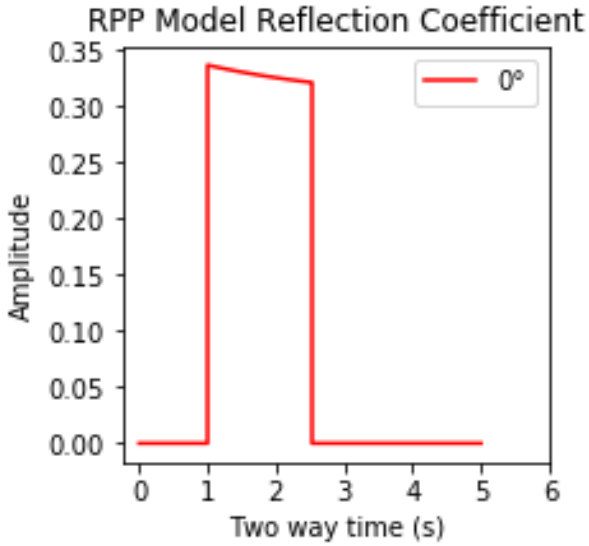

Figure 2.22. RPP reflection coefficient response for model 3 parameters at vertical incidence.

rate, I interpolated the RPP result using a linear one dimensional interpolation to match the Ricker wavelet sampling. Then, I convolved the RPP response (Figure 2.22) with the Ricker wavelet in the time domain to get figure 2.23.

I immediately noticed some interesting results. The waveforms representing the top and bottom of the transition zone have a different shape than the Ricker wavelet. To get a better understanding of my results, I compared the input Ricker wavelet amplitude response with the top of the transition zone amplitude response (Figure 2.24) in the frequency domain. I applied a Fast Fourier Transform to convert the data from the time domain to the frequency domain and I got figures 2.25 and 2.26. Then, I plotted both frequency responses in the same plot for a better comparison (Figure 2.27).

I noticed that the top of the transition zone max amplitude is almost double the Ricker wavelet max amplitude. I applied a spectral ratio in the frequency domain between the Ricker wavelet and the top of the transition zone result to

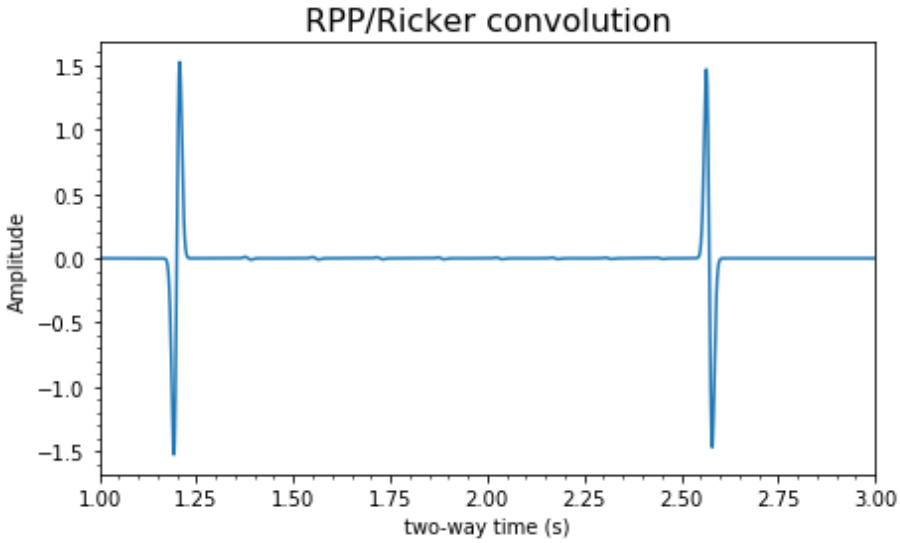

Figure 2.23. Seismic response in the time domain from the convolution of the RPP equation results with a Ricker wavelet which shows a half Ricker wavelet shape response for the top and bottom of the transition zone and small amplitude signals representing the transition zone layers.

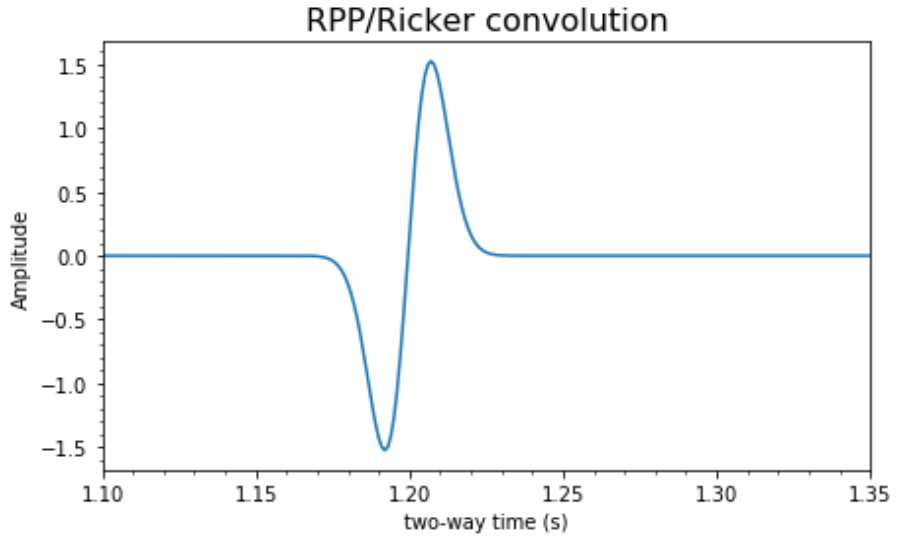

Figure 2.24. A closer look at the top of the transition zone seismic response in the time domain from the convolution of the RPP equation result with the Ricker wavelet which shows a half Ricker wavelet shape response.

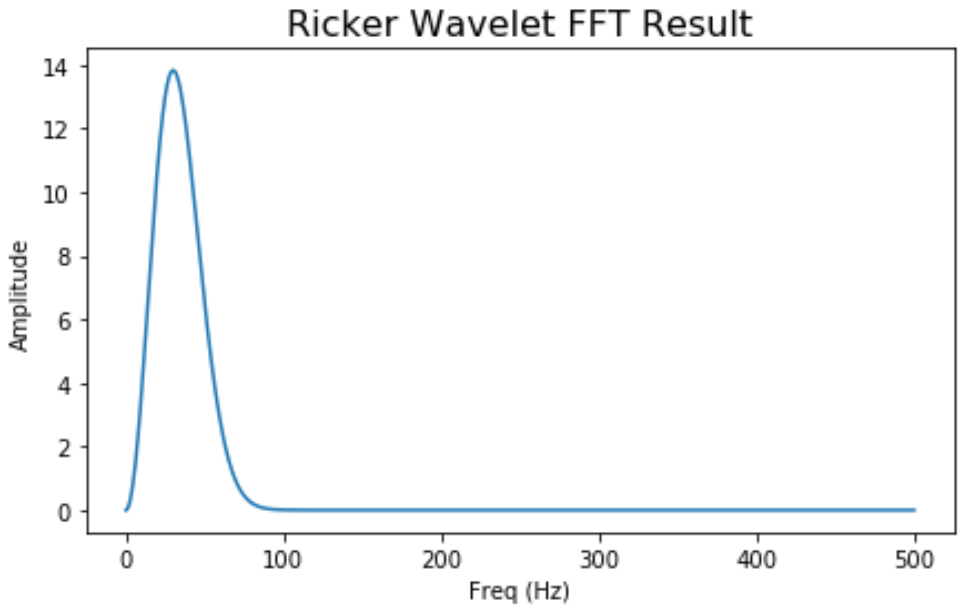

Figure 2.25. Fast Fourier Transform of the Ricker wavelet illustrating the true frequency range (Nyquist Frequency) from 0 to 500 Hz and a maximum amplitude of almost 14.

get the plot in figure 2.28. The plot shows a linear line from 0 to 80 Hz which indicates that the RPP response is an integration of the Ricker wavelet. To verify this, I multiplied the Ricker wavelet by $i\omega$ which produced a similar result to the response in figure 2.24.

This integral response is due to the fact that the Primary Pulse Method accounts for gradual changes in elastic parameters as the wave moves through the transition zone. Since the layers in the transition zone are closely packed and the differences in elastic parameters between them are small, the layer reflection responses are almost nullified. However, since there are no responses before or after the transition zone, I got a half Ricker wavelet response for the top and bottom of the transition zone.

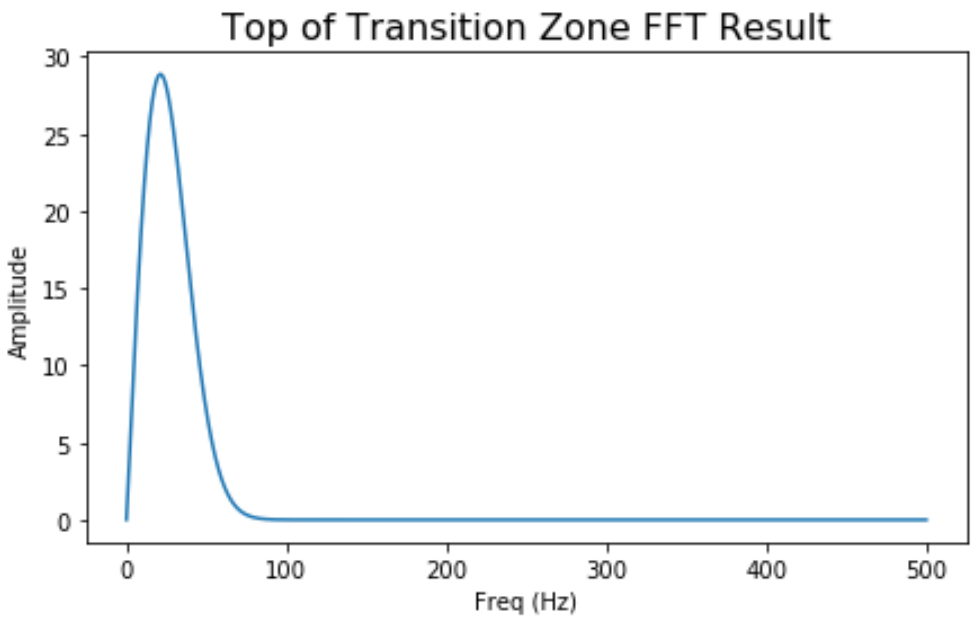

Figure 2.26. Fast Fourier Transform of the top of the transition zone response illustrating the true frequency range from 0 to 500 Hz and a maximum amplitude of almost 30.

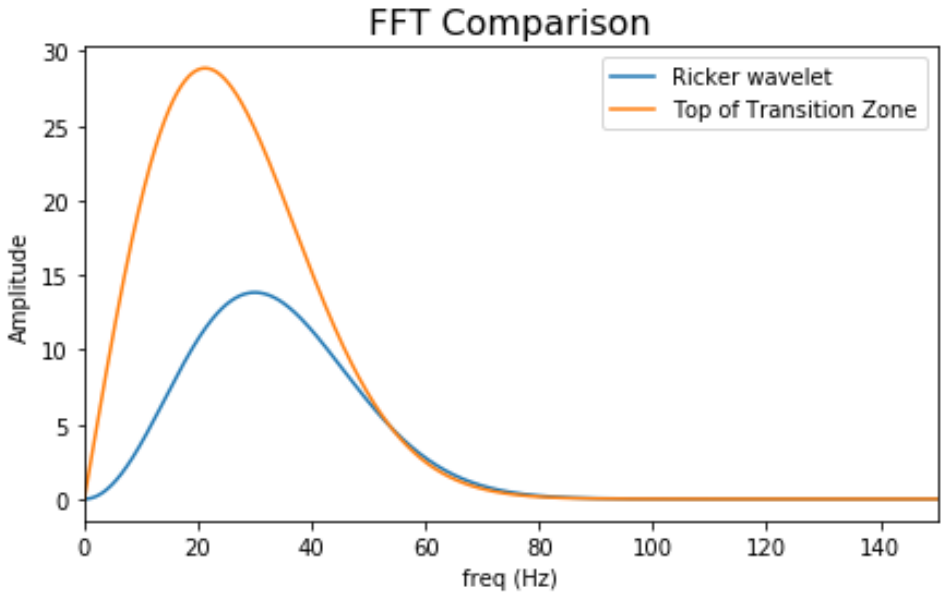

Figure 2.27. Fast Fourier Transform comparison between the top of the transition zone response and the Ricker wavelet. The top of the transition zone response max amplitude is almost double the Ricker wavelet max amplitude.

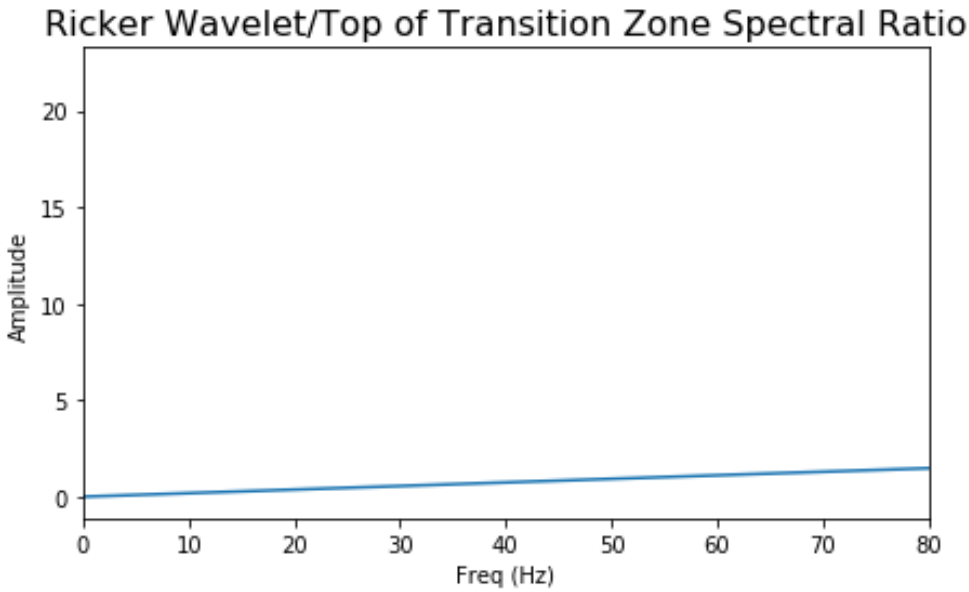

Figure 2.28. Spectral Ratio between the top of the transition zone response and the Ricker wavelet. The plot shows a linear line from 0 to 80 Hz.

2.4 The Primary Pulse Method vs. Acoustic Impedance

I got an interesting result when convolving the Ricker wavelet with the RPP response but how does this result compare to other reflection coefficient methods? and what differences would arise in amplitudes and wavelet shapes? To answer these questions, I compared the RPP equation with the Convolution Method of Acoustic Impedance.

Acoustic impedance is defined as the product of compressional velocity with density. Its reflection coefficient equation is defined as the differences in velocities and densities between two seismic interfaces in the subsurface (2.6) (Aki and Richards (1980), Mahmoudian and Margrave (2007), Sheriff and Geldart (1995)).

$$R = \frac{Z_2 - Z_1}{Z_2 + Z_1} \tag{2.6}$$

where:

$Z_1 = \alpha_1\rho_1$, $Z_2 = \alpha_2\rho_2$

α= compressional velocity, ρ= density. $_1$, $_2$ denote first and second medium respectively.

I convolved the Acoustic Impedance reflection coefficient (Figure 2.29) with the same Ricker wavelet, velocities, sampling rate and number of samples I applied for the RPP convolution. I used the same densities for the top and bottom layers (2 gm/cc, 3.5 gm/cc respectively) and I chose a density of 3 gm/cc for the transition zone.

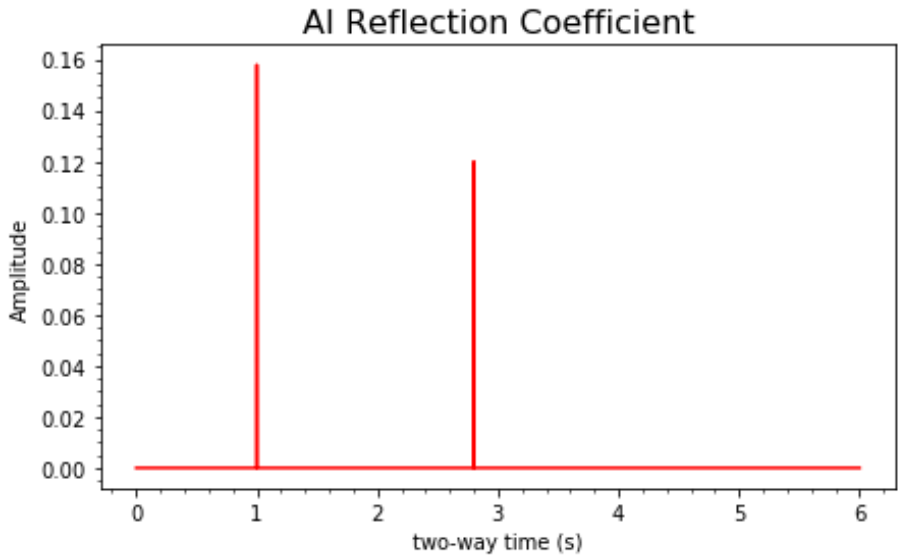

Figure 2.29. The Acoustic Impedance reflection coefficient responses where the top and bottom of the transition zone appear as spikes

After inputting my parameters and applying the convolution, I got the response in figure 2.30.

Examining the responses of both methods (Figures 2.23, 2.30), they appear similar in arrival time but different in amplitude and shape. This is because Acoustic Impedance applies sudden changes in elastic parameters instead of gradual changes as seen with the RPP equation (Figure 2.31). That is why the top and bottom transition zone reflections seen here both appear as Ricker wavelets but appear integrated in the RPP response. The difference in wavelet shape between the two methods raises a couple of interesting questions. What effect would the RPP response have when applied to a transition zone with a smaller thickness? What would be the implications of using this method on thin layers where tuning would occur? How will the shape of the wavelet affect tuning and what responses would be seen from applying the Primary Pulse Method on well log data?

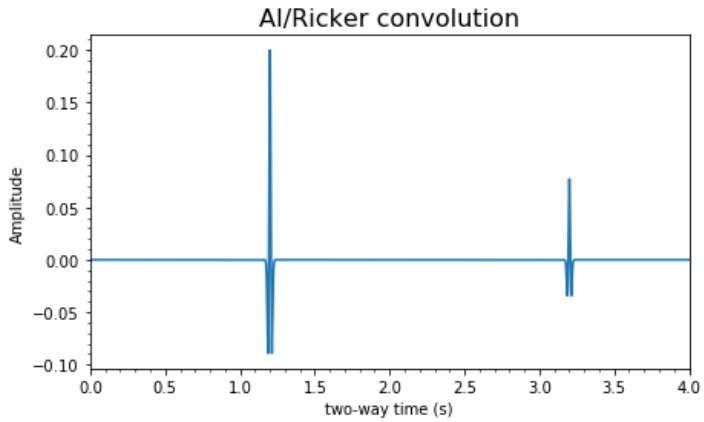

Figure 2.30. Seismic response in the time domain from the convolution of Acoustic Impedance with a Ricker wavelet which shows Ricker wavelet waveform responses for the top and bottom of the transition zone.

Figure 2.31. Primary Pulse Method and Acoustic Impedance model comparison. The ray path in the transition zone for the Primary Pulse Method accounts for gradual changes in elastic parameters, while the ray path in Acoustic Impedance accounts for sudden changes in elastic parameters.

Chapter 3

THE APPLICATION OF THE PRIMARY PULSE METHOD ON THIN LAYERS, AVO ANALYSIS AND WELL LOG DATA

3.1 The Application OF The Primary Pulse Method on Thin Layers

Richards and Frasier (1976) implemented the Primary Pulse Method on a thick transition zone but what will be the effect of implementing it on thin layer cases?

To investigate this effect, I applied the RPP equation on a small transition zone to examine the responses in the existence of thin layers; which are usually present

in real seismic data (Bakke and Ursin (1998), Farfour *et al.* (2017), Foster and Keys (1999), Foster *et al.* (2010), Widess (1973)).

For my investigation, I compared the responses of the RPP equation and Acoustic Impedance using a small transition zone of 50 m which is divided into 10 layers with a transition zone density of 2.75 g/cc for Acoustic Impedance (3.1 and 3.2).

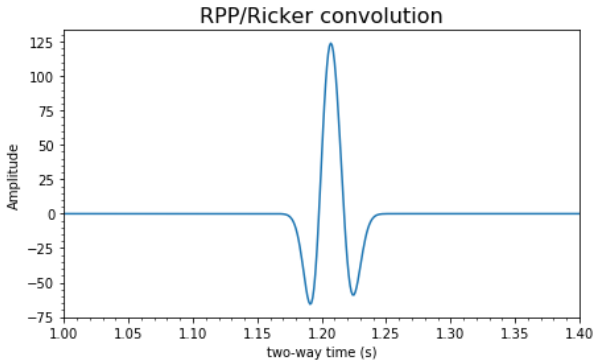

Figure 3.1. Seismic response in the time domain from the convolution of the RPP responses with a Ricker wavelet (50m transition zone).

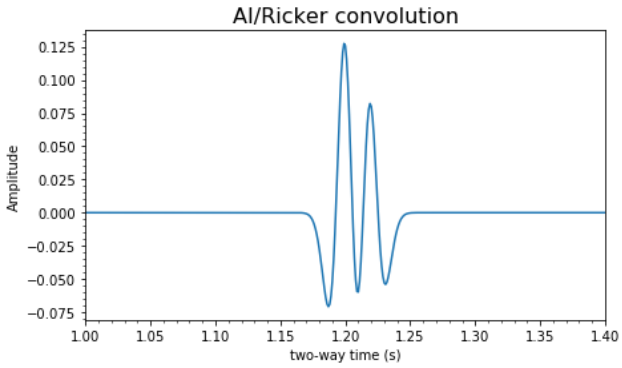

Figure 3.2. Seismic response in the time domain from the convolution of Acoustic Impedance with a Ricker wavelet (50m transition zone).

The plots show that the top and bottom boundaries interfere with each other (tuning). However, because of the difference in the waveform shapes, the RPP response appears as one wavelet while the acoustic impedance response shows two

wavelets separating. Both plots have higher amplitudes than the 5 km transition zone case but the RPP result shows unrealistic high amplitudes.

To get a better understanding of the effects of thin layers on the RPP equation, I used tuning curves. These curves show the effect of changing layer thickness on amplitude responses and can help in identifying rock lithology, hydrocarbons and geophysical properties (Chopra *et al.* (2006), Chung and Lawton (1999), Simm (2009)).

Figures 3.3 and 3.4 show the tuning curves for thicknesses from 10 m to 300 m with a 10 m increment. I chose the peak amplitude for every increment to be plotted against thickness.

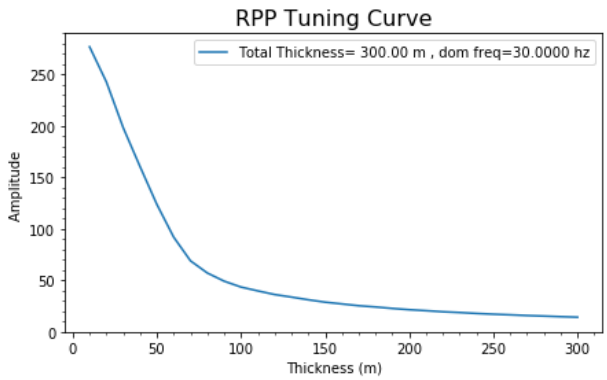

Figure 3.3. Tuning curve for RPP that shows thicknesses from 10 m to 300 m with 10 m increments plotted against max amplitude. As thickness increases, amplitude decreases because as the integrated wavelet responses separate, they will not interfere with each other.

The plots show some notable differences. First, the Acoustic Impedance plot (figure 3.4) shows reasonable amplitude values while the RPP (figure 3.3) shows unrealistic high amplitudes as thickness decreases. This is because as thickness goes to zero, the elastic parameter derivatives in the RPP equation go to infinity. The second difference to note is in the Acoustic Impedance plot where as thickness increases, amplitude decreases before increasing until it reaches a constant value.

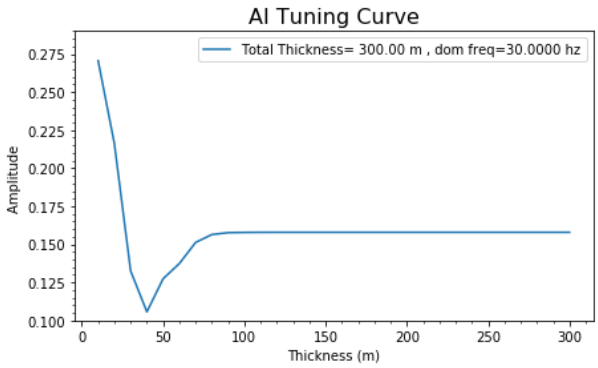

Figure 3.4. Tuning curve for Acoustic Impedance that shows thicknesses from 10 m to 300 m with 10 m increments plotted against max amplitude. As thickness increases, amplitude decreases then starts increasing due to destructive and constructive wave interference. The amplitude reaches a constant value when the waves completely separate.

This is due to interference between the top and bottom responses of the transition zone, where constructive and destructive interference occurs until they completely separate; which is when the amplitude reaches a constant value. In contrast, the RPP response shows high amplitudes at small thicknesses then decreases to an almost constant value as thickness increases. This is due to the top and bottom responses appearing as half Ricker wavelet shapes (integrals of the Ricker wavelet) so their opposite lobes will not interfere with each other as thickness increases.

I believe that the unrealistic high amplitudes in the Primary Pulse Method for thin layer cases is due to ignoring multiples. To investigate this effect, I compared the Primary Pulse Method with a method that considers the effect of multiples called the Reflectivity Method.

3.2 The Reflectively Method

The Reflectivity Method calculates the wave-field of a layered media in the frequency domain using a matrix that takes into account all ray paths in the reflection zone (Kennett (1975), Kind (1976), Kennett and Clarke (1983)). Throughout the years, the Reflectivity Method underwent developments to deal with a number of limitations that include attenuation, source and receiver locations (on the surface or buried) and structure differences at the source and receiver. Fuchs and Müller (1971), Kennett (1975), Kind (1976), Stephen (1977), Kennett (1979), Kennett (1980), Fryer (1980), Kennett and Illingworth (1981), Kennett and Clarke (1983), Sipkin *et al.* (1978), O'neill and Hill (1979).

Although the Reflectivity Method helps in understanding the Earth's structure, it is not used frequently for modeling and seismic interpretation because it is limited by long computational times. This computation slowness is affected by the number of samples, the use of long frequency series and the approximation of a velocity gradient based on the number of thin layers (Braile and Smith (1975), Spudich and Orcutt (1980a), Spudich and Orcutt (1980b), Kempner and Gettrust (1982a) Kempner and Gettrust (1982b)).

The Reflectivity Method implements the system of equations of the form

$$\partial_z b = -i\omega A b + g, \tag{3.1}$$

where:

$\partial_z b$= Partial derivative of the physical variables with respect to depth

ω= Frequency

A= Matrix with elastic constants depending on homogeneous media properties, horizontal slowness and frequency. (2x2 Matrix for azimuths direction of motion or 4x4 for radial and vertical direction of motion)

b= The physical variables of a plane wave

g= source function

then by applying an inverse Fourier-Hankel transform on 3.1 the result is the expression

$$u(x,\omega) = \int_0^\infty \omega^2 p \quad dp \quad u^{\sim}(\omega,p) \quad J_0(\omega p x), \tag{3.2}$$

where:

$u(x,\omega)$ = displacement vector in the frequency domain

x = Reciever distance from source

ω = raidan temporal frequency frequency

p = horizontal slowness

dp= slowness derivative

$u^{\sim}(\omega,p)$ = reflectivity function

J_0 = Zero order Bessel function

The reflectivity function here represents the summation of plane waves through homogeneous layers with different slowness in the frequency domain.

The last step is to apply an Inverse Fourier Transform on equation 3.2 to get the equation

$$u(x,t) = \frac{1}{2\pi} \int_{-\infty}^{\infty} d\omega \quad e^{-i\omega t} \quad u(x,\omega), \tag{3.3}$$

which gives the reflectivity results in the time domain (Mallick and Frazer (1987)).

The Reflectivity Method equation I used is calculated based on Stovas and Ursin (2003). The method was coded by Yuriy Ivanov and Georgios Papageorgiou Papageorgiou and Ivanov (2018-2019). Although they applied the code on a Vertically Transverse Isotropic (VTI) medium, I applied it on a homogeneous isotropic medium.

The Reflectivity Method calculates the reflection coefficients of incident plane waves reflected or transmitted from subsurface layers. I used a propagating wavefront source for my testing which the method expresses as a number of plane waves reflecting off the layers of the transition zone at different angles. This will result in reflections bouncing between layers. So the Reflectivity Method considers the effect of multiples.

First, I calculated the elastic parameters at each layer using a matrix multiplication. Then, I computed the reflection coefficients in the frequency domain for each layer as a number of plane waves and summed up the reflection coefficients into one value. I then convolved these reflection responses with a Ricker wavelet in the frequency domain and finally applied a Fast Fourier Transform to convert the results to the time domain.

For my testing, I used a transition zone with a specified thickness between two half

spaces. The transition zone consists of a number of layers with equal thicknesses that sum up to the total transition zone thickness.

I plotted the Reflectivity Method using the same elastic parameter values as the RPP equation to examine the effects of thickness and number of layers on the reflection result. All my tests used a constant P-wave velocity of 5 km/s, a constant SV-wave velocity of 3 km/s, a top half space density of 2 gm/cc, a bottom half space density of 3.5 gm/cc and a gradual change in density. All tests include two half spaces (top and bottom), a transition zone, a source and receiver depth of 3 km under the surface and a 30 Hz Ricker wavelet.

My first test was a single layer transition zone with a thickness of 1 km (Figures 3.5 and 3.6). The figures show one reflection corresponding to one layer in the transition zone.

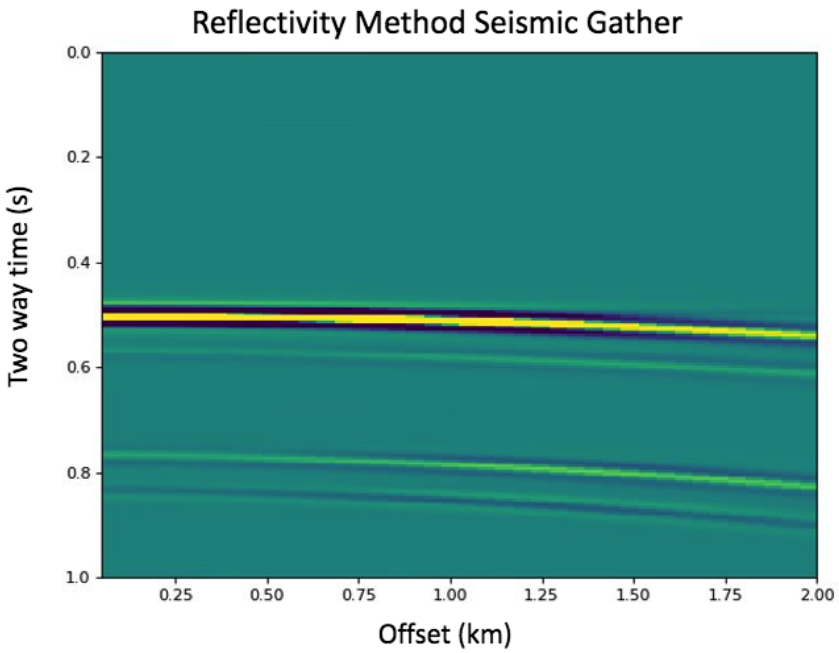

Figure 3.5. Seismic gather showing the result of the Reflectivity Method for the case of a 1-layer 1 km transition zone.

Next, I tested the effect of increasing the number of layers. I used a transition

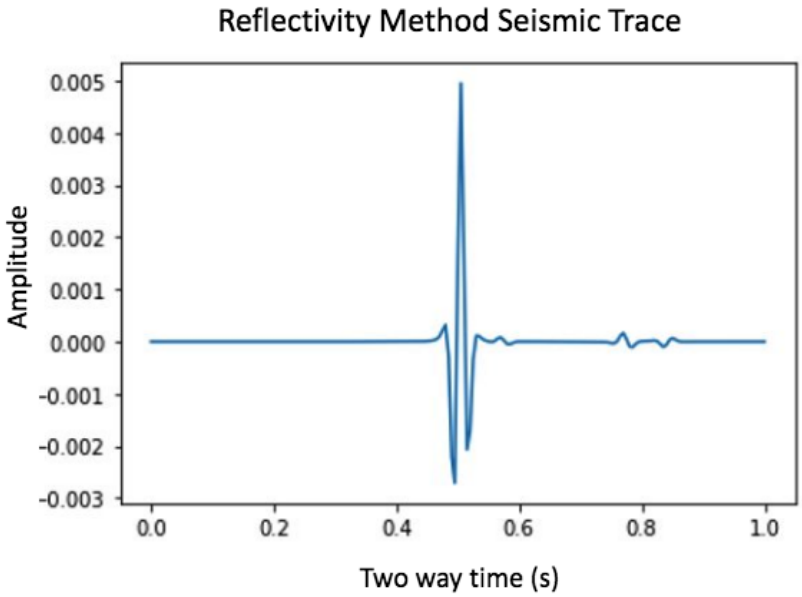

Figure 3.6. Seismic trace showing the result of the Reflectivity Method for the case of a 1-layer 1 km transition zone.

zone of 1 km but this time I divided the transition zone into 5 layers and got figures 3.7 and 3.8. By comparing figures 3.5 and 3.7, it can be seen that the 1 layer transition zone produces one reflection and the 5-layer transition zone produces 5 reflections. This observation can also be seen when comparing the seismic trace from each case (Figures 3.6 and 3.8).

Note that the amplitudes for both cases are very similar. This is a result of including multiples in the Reflectivity Method calculations.

Next, I tried a 5-layer transition zone with a thickness of 500 m (Figures 3.9 and 3.10). Again, I saw similar results when comparing these plots with the 1 km thick transition zone (Figures 3.7 and 3.8).

I then increased the number of layers to 10 layers and got the responses in figures 3.11 and 3.12. Although I used 10 layers, I did not see any reflections between the top and bottom of the transition zone but I did notice 10 multiples in the seismic

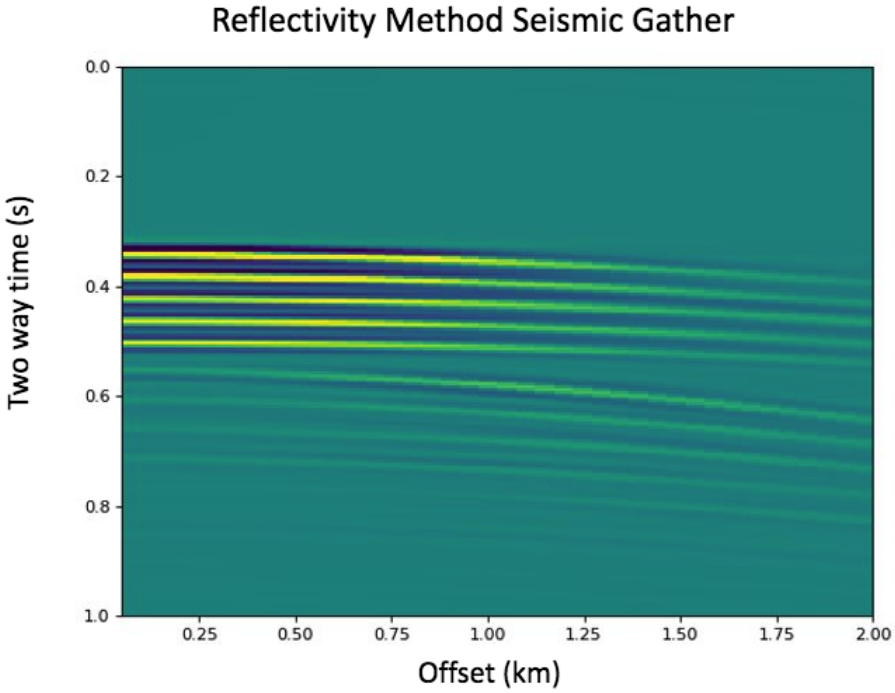

Figure 3.7. Seismic gather showing the result of the Reflectivity Method for the case of a 5-layer 1 km transition zone.

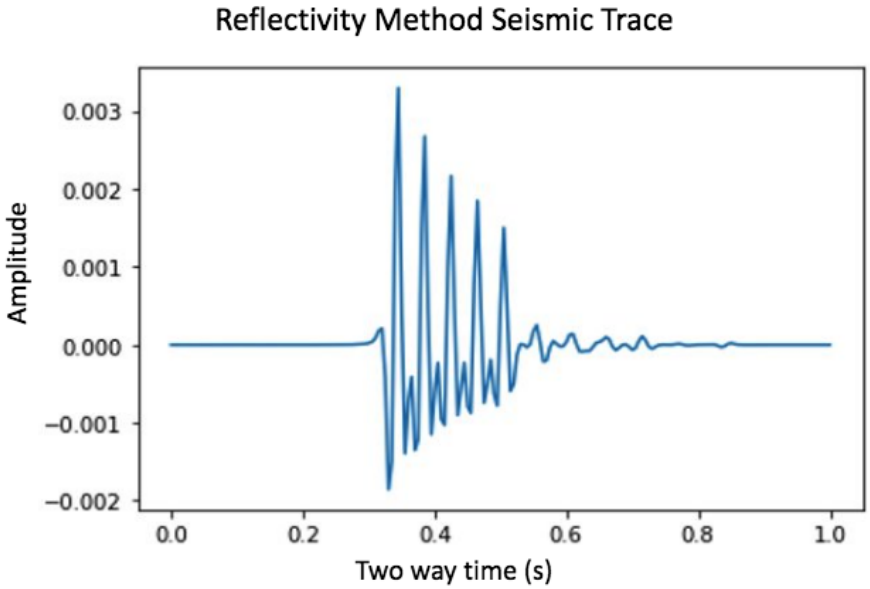

Figure 3.8. Seismic trace showing the result of the Reflectivity Method for the case of a 5-layer 1 km transition zone.

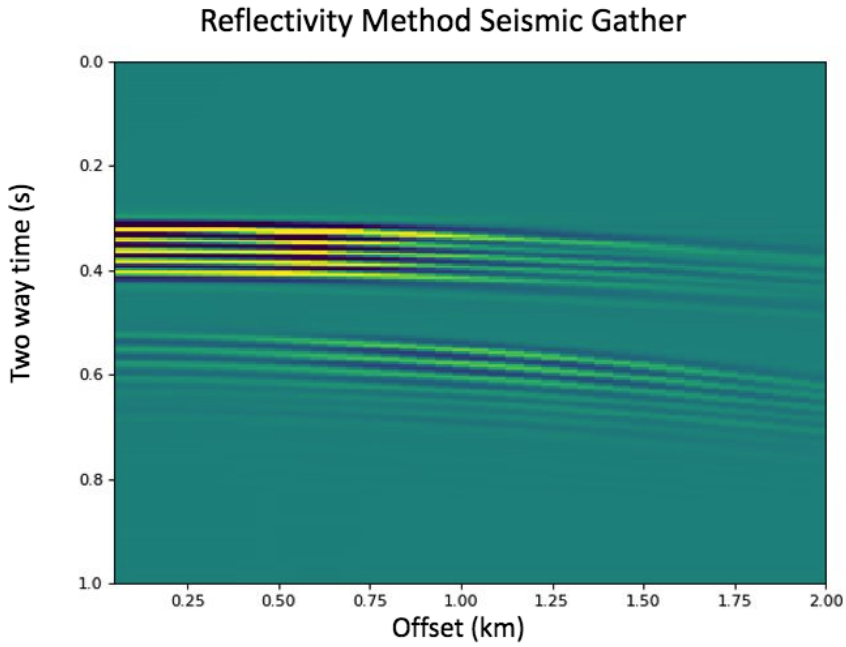

Figure 3.9. Seismic gather showing the result of the Reflectivity Method for the case of a 5-layer 500 m transition zone.

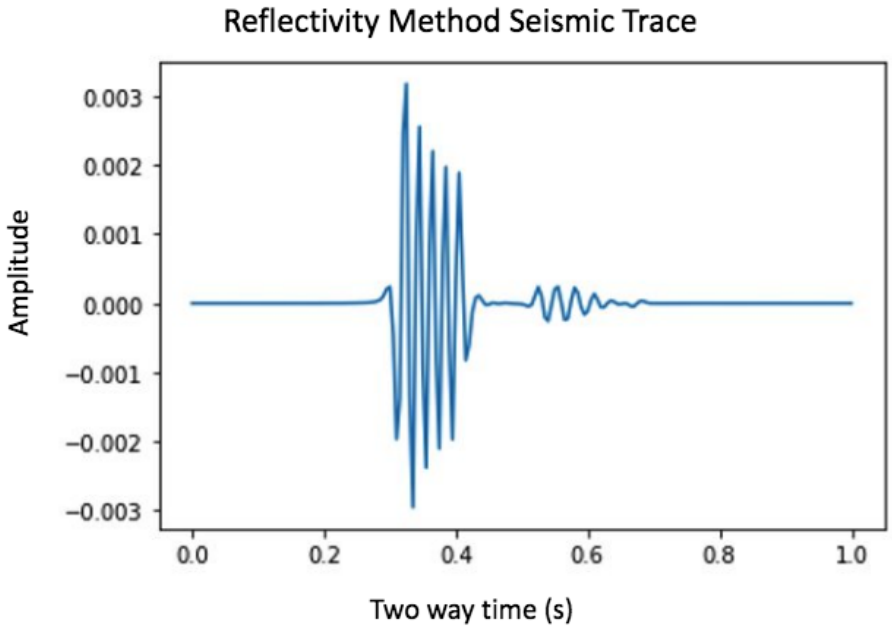

Figure 3.10. Seismic trace showing the result of the Reflectivity Method for the case of a 5-layer 500 m transition zone.

gather (Figure 3.11. An important fact to note in the 10 layer case is how the top and bottom reflections of the transition zone appear as half Ricker wavelet shapes (integrated wavelet) similar to the RPP response (Figures 3.12 and 3.13. This solidifies that the RPP gave correct reflection responses.

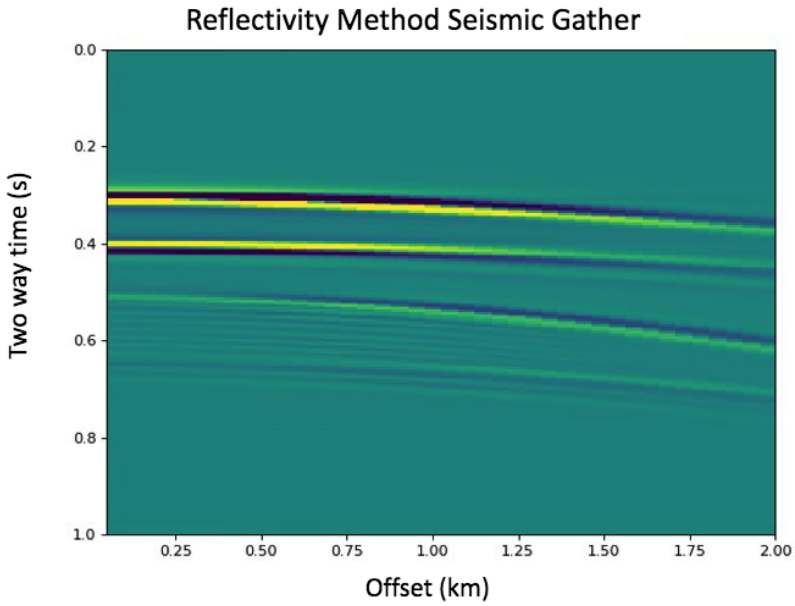

Figure 3.11. Seismic gather showing the result of the Reflectivity Method for the case of a 10-layer 500 m transition zone.

Next, I increased the number of layers in the transition zone to 100 layers and got figures 3.14 and 3.15. Although I increased the number of layers to 100, the results show a similar but smoother response compared to the 10 layer case which indicates using 10 layers is sufficient for the comparison with the RPP response.

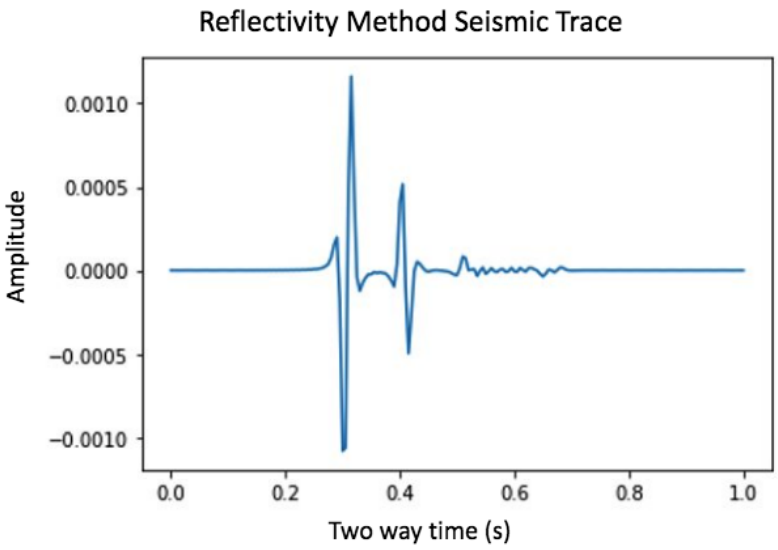

Figure 3.12. Seismic trace showing the result of the Reflectivity Method for the case of a 10-layer 500 m transition zone.

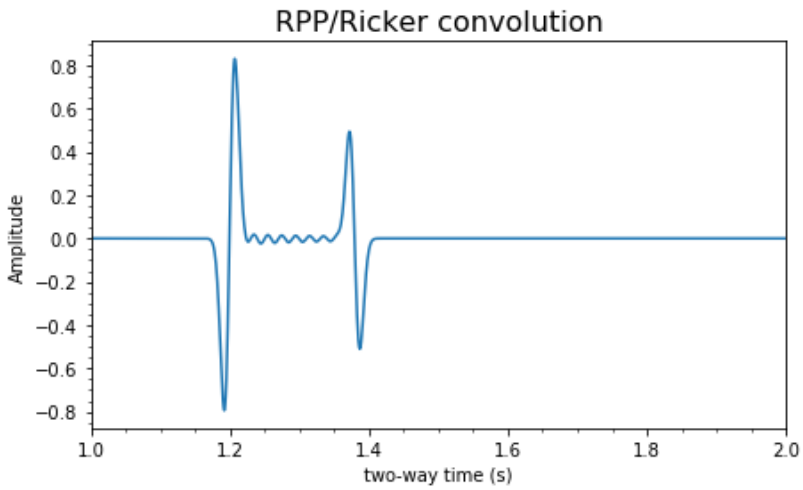

Figure 3.13. Seismic trace showing the result of the RPP equation for the case of a 10-layer 500 m transition zone.

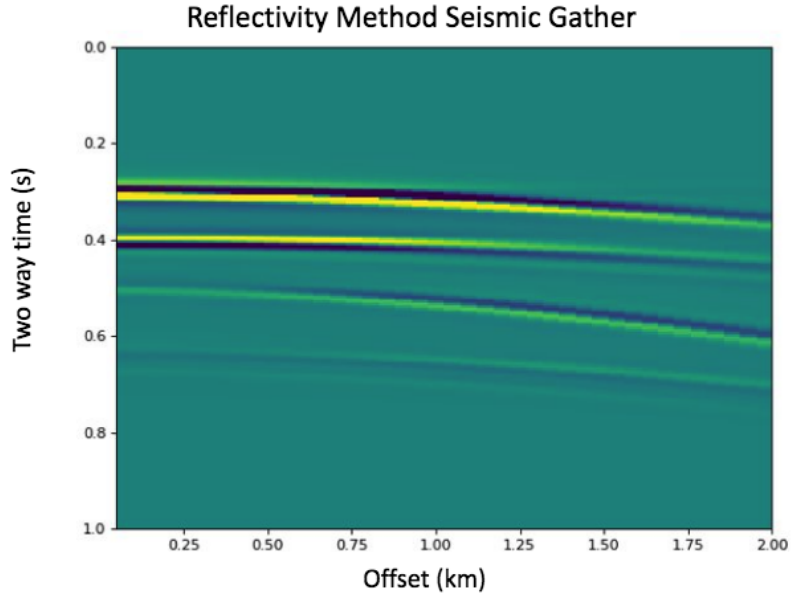

Figure 3.14. Seismic gather showing the result of the Reflectivity Method for the case of a 100-layer 500 m transition zone.

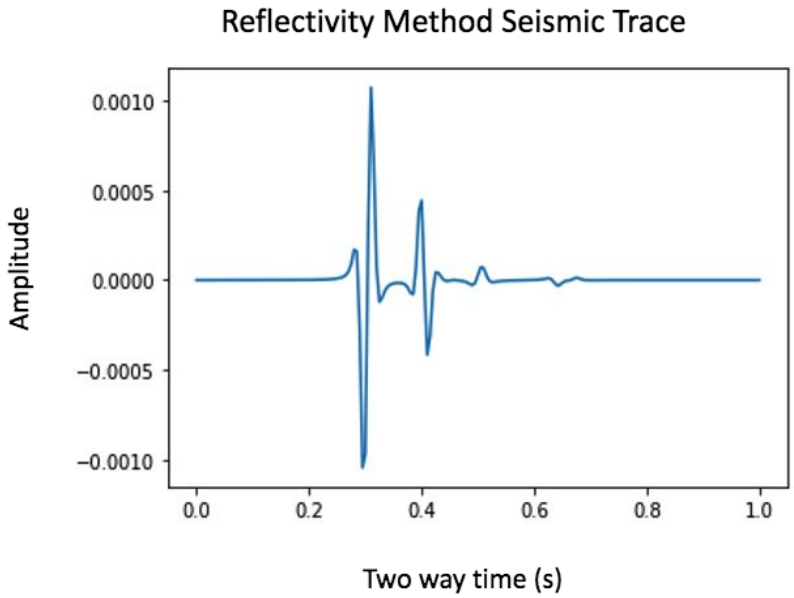

Figure 3.15. seismic trace showing the result of the reflectivity method for the case of a 100-layer 500m transition zone.

For my next testing, I examined the effect of tuning on the Reflectivity Method. I decreased the thickness to 80 m for the 5-layer case. The results here (figures 3.16 and 3.17) look different compared with the 500 m thickness results (figures 3.9 and 3.10). With an 80 m thickness transition zone, the tuning effect is present. The seismic gather shows only one reflection and one multiple. The seismic trace shows one wavelet which is actually two wavelets that appear as one due to tuning and it also shows one multiple. I then decreased the thickness to 50 m to get figures 3.18 and 3.19. Due to the tuning effect note a small increase in amplitude for the 50 m case.

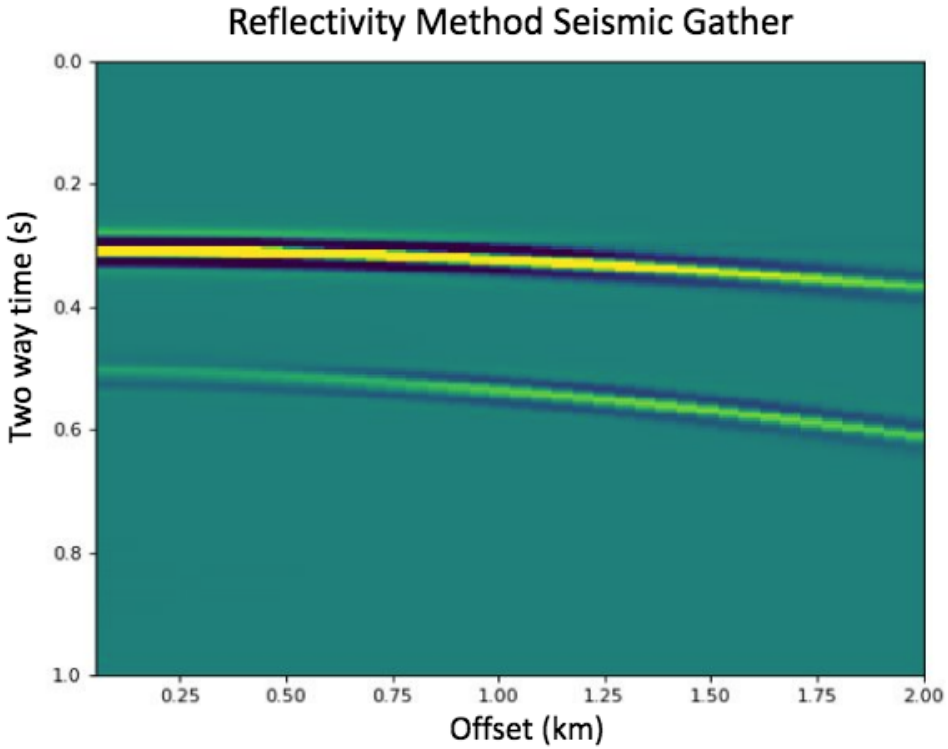

Figure 3.16. Seismic gather showing the result of the Reflectivity Method for the case of a 5-layer 80 m transition zone.

Finally, I produced tuning curves for the Reflectivity Method to see the effect of thickness on amplitude. I used the 5-layer and 10-layer cases to produce a tuning curve for thicknesses from 0 m to 100 m with a 10 m increment. I got the plots in figures 3.20 and 3.21. From these tuning curve plots and contrary to the RPP

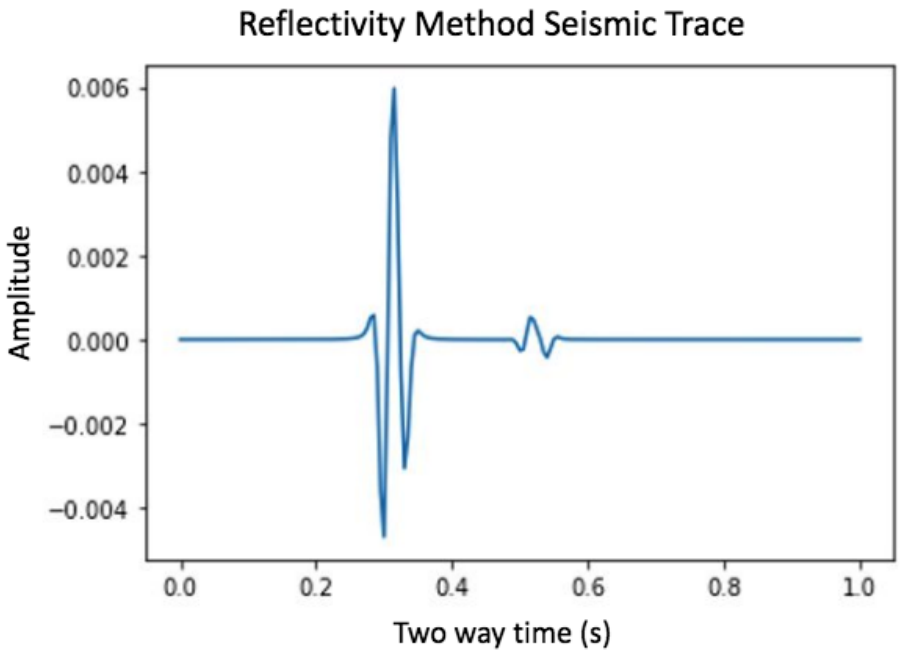

Figure 3.17. Seismic trace showing the result of the Reflectivity Method for the case of a 5-layer 80 m transition zone.

tuning curves, the amplitude does not go to infinity as thickness goes to zero. This outcome supports my belief that ignoring multiples in the Primary Pulse Method results in unrealistic amplitude values in thin layer cases.

Although the Primary Pulse Method fails theoretically for thin layer cases, I applied the method on well log data to investigate if this limitation would be relevant in real seismic data.

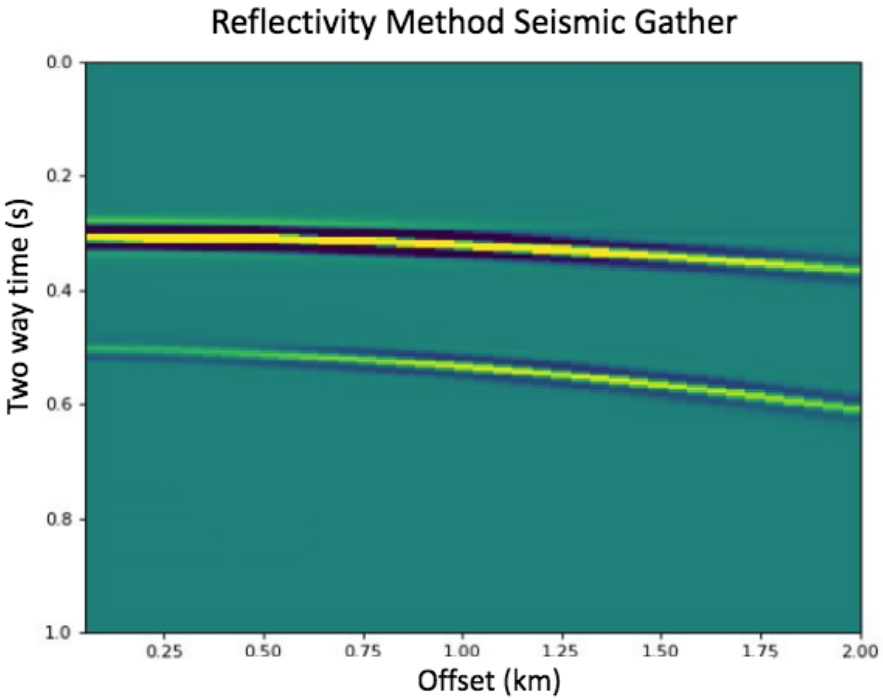

Figure 3.18. Seismic gather showing the result of the Reflectivity Method for the case of a 5-layer 50 m transition zone.

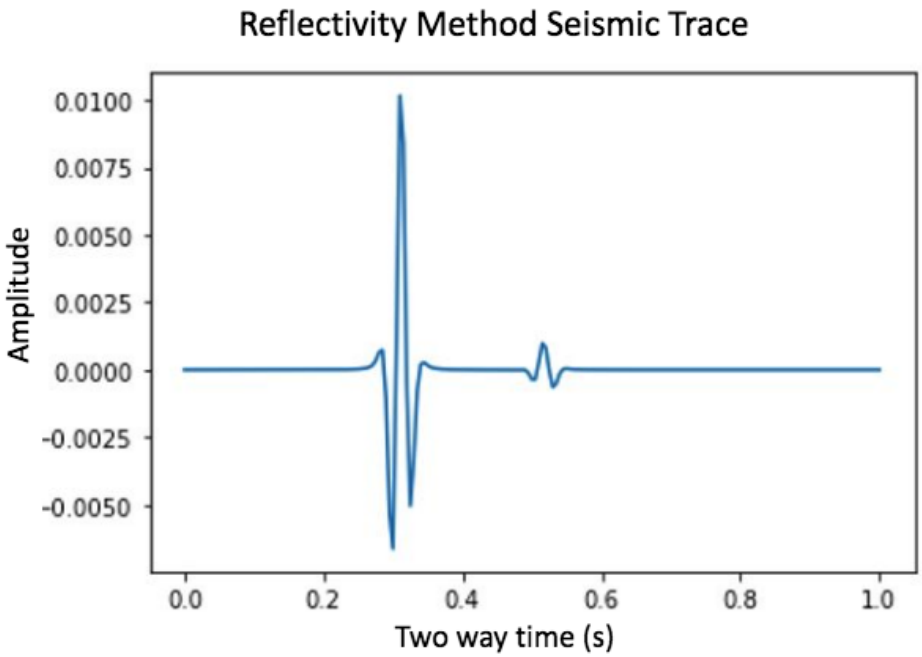

Figure 3.19. Seismic trace showing the result of the Reflectivity Method for the case of a 5-layer 50 m transition zone.

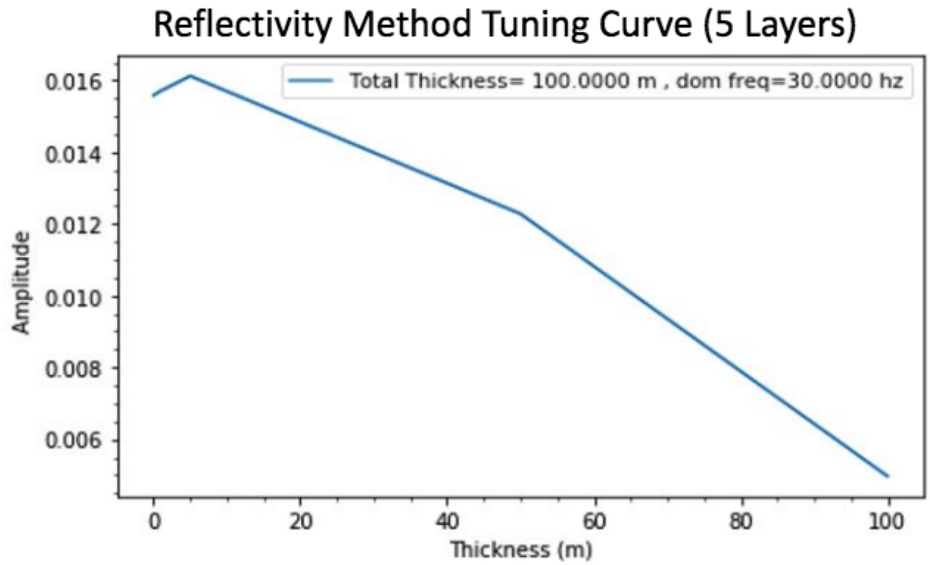

Figure 3.20. Tuning curve for the Reflectivity Method results for a 5-layer transition zone from 0 m to 100 m.

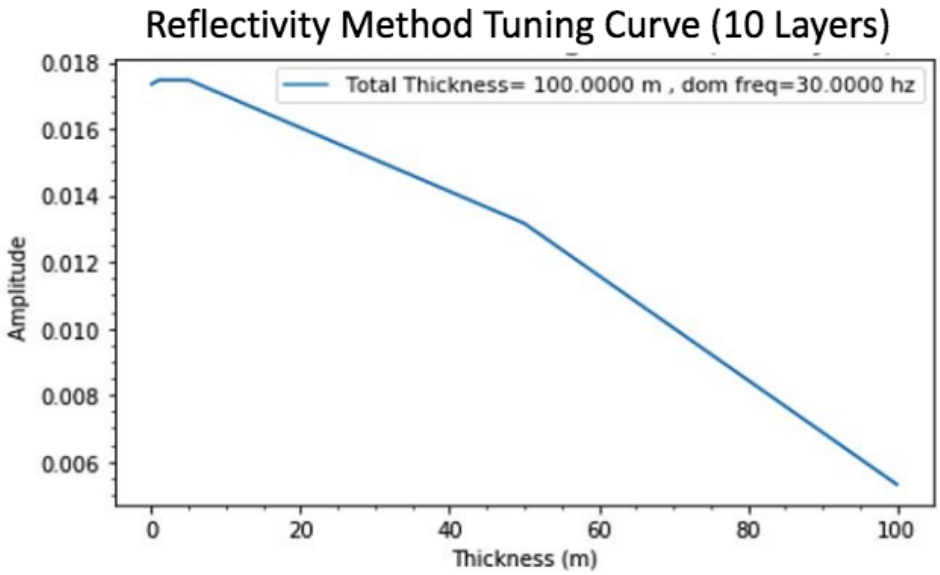

Figure 3.21. Tuning curve for the Reflectivity Method results for a 10-layer transition zone from 0 m to 100 m.

3.3 The Application of The Primary Pulse Method on Well Log Data

When I applied the RPP equation on thin layers I discovered that it results in unrealistic amplitude responses which indicates that the theory behind the Primary Pulse Method is flawed. However, would this shortcoming affect real seismic data? To answer this question, I applied the RPP equation to well log data and examined the amplitude responses.

I was provided with well log data from North America for testing. This data shows velocities, densities and depth measurements. I converting depth to two-way travel time using layer thickness and P-wave velocity
(t= 2*(layer-thickness/Vp) (Figure 3.22).

I used the well log data to compare the RPP equation with the Shuey (1985)

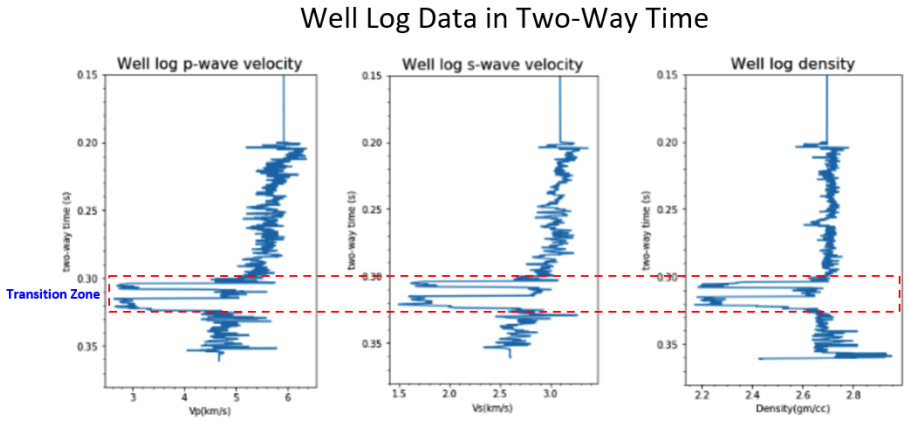

Figure 3.22. Well log elastic parameters plotted for two-way time. P-wave velocity on the left, SV-wave velocity in the middle and density on the right.

equation at vertical incidence. My testing was done in the time domain with an incident angle of 0° and I got the responses in figures 3.23 and 3.24.

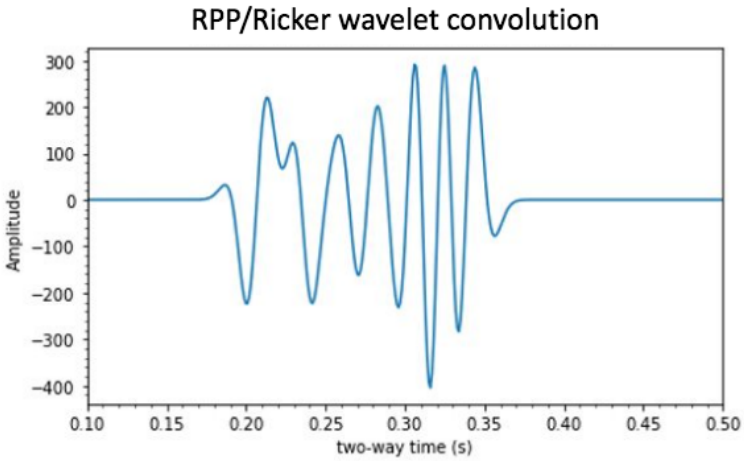

Figure 3.23. Seismic response in the time domain from the application of the RPP equation on well log data for vertical incidence.

Both equations showed similar waveform responses at the beginning of the data with more pronounced differences as the wave travels through the well log; specially in the transition zone (between 0.31-0.34 seconds). However, I still got unrealistic high amplitudes for the RPP responses. These results agree with

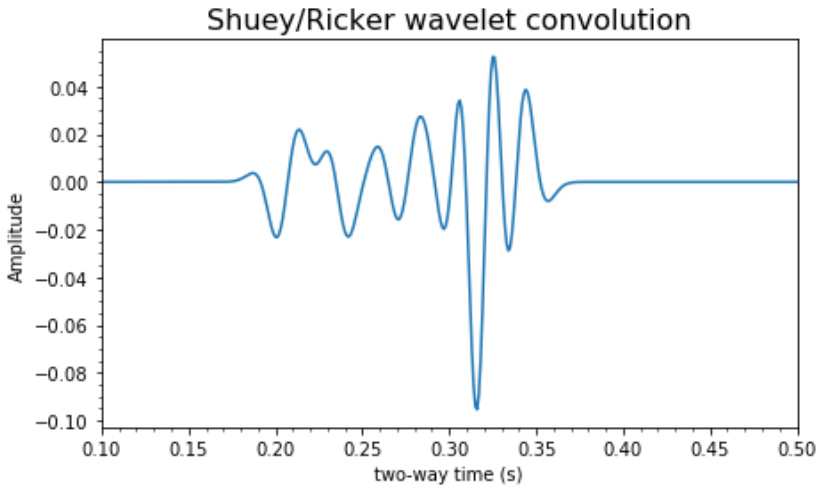

Figure 3.24. Seismic response in the time domain from the application of the Shuey (1985) equation on well log data for vertical incidence.

the results I got from the thin layer model testing and confirms that the Primary Pulse Method should not be used for thin layer cases.

Although the Primary Pulse Method fails theoretically and practically, one of its advantages is considering the effect of ray bending. This raises the question of how much will ray bending affect seismic data?

To answer this question, I compared the responses of the Shuey (1985) method on AVO analysis with and without accounting for ray bending.

3.4 The Effect of Ray Bending on AVO Analysis

To understand the impact of ray bending on AVO analysis, I used the well log data from North America to produce traces for different angles of incident. I plotted the traces for the incident angles from 0° to 30° with an increment of 1° for each trace.

For my testing, I chose the Shuey (1985) equation as the main reflection coefficient equation with the time series equation as the conversion of layer depth to two-way time. I implemented Shuey (1985) equation in two forms, one will be using a constant angle of incidence as the wave moves through the well log (no ray bending) and the other will be using a variable angle of incidence as the wave moves through the well log (ray bending). To calculate the angle of incidence for ray bending at each layer, I used Snell's law and slowness ($\theta = \arcsin(s * \alpha)$).

My testing produced the plots in figures 3.25 and 3.26 that show seismic responses of 30 angles of incidence from 0° to 30° with each trace represented as one angle of incidence.

The synthetic data plots show very similar results with slight changes in amplitude as the angle of incidence increases. The slight changes in amplitude are mostly seen around the well log transition zone (between 0.31 - 0.34 seconds) (Figure 3.27).

For a better understanding of these changes in amplitude, I plotted the average amplitudes of the well log data transition zone in relation to the angle of incidence of each trace (Figure 3.28).

Examining figure 3.28 shows a gradual and more subtle increase in amplitude when applying ray bending compared to a fast increase in amplitude without ray bending. This shows that the effect of ray bending as considered by Richards and Frasier (1976) has an important impact on AVO analysis and shows the potential of attaining different seismic responses with ray bending.

Next, I compared the responses of the Shuey (1985) equation with and without ray bending vs. the Reflectivity Method to evaluate how well they agree with each other.

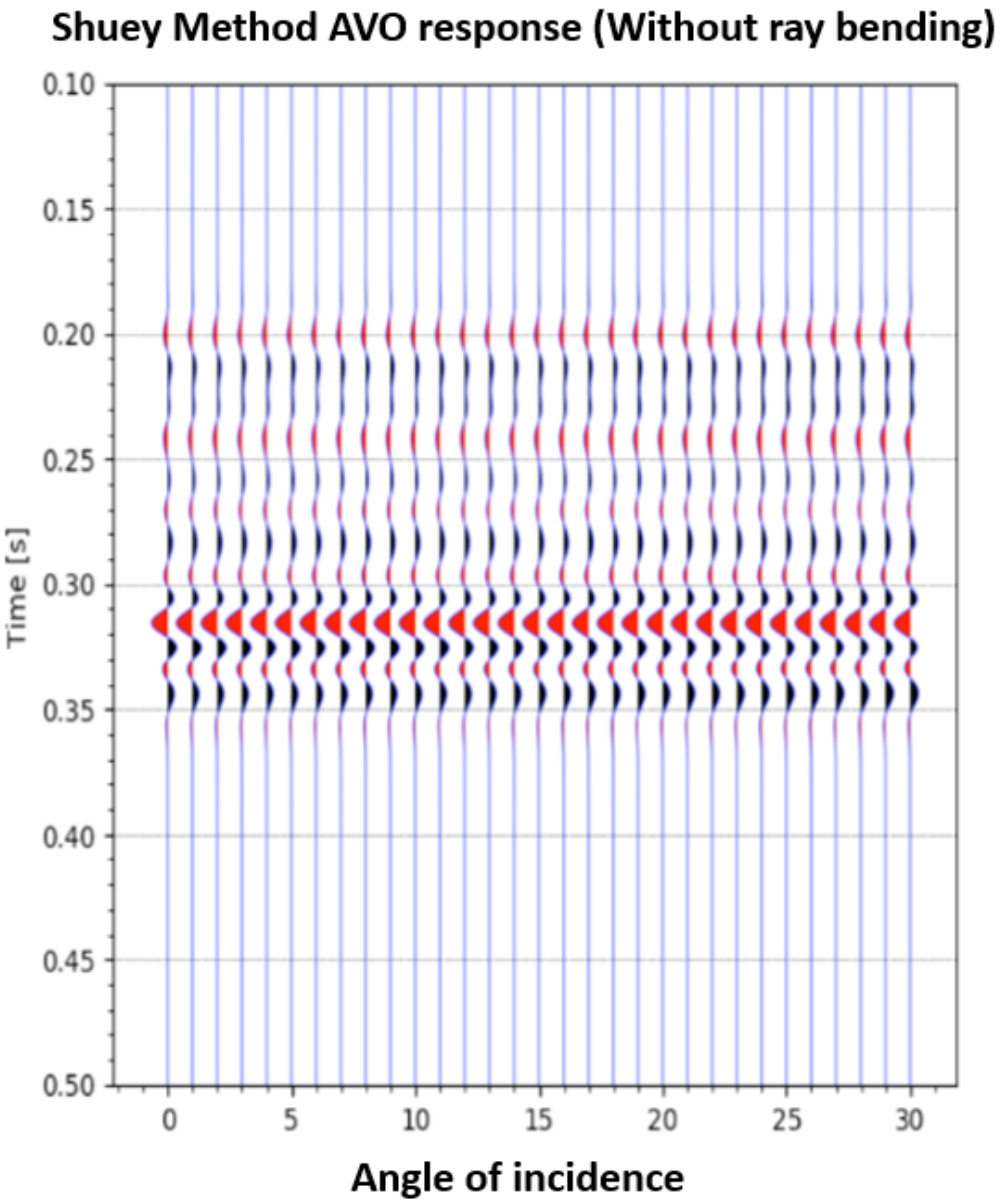

Figure 3.25. Synthetic data that shows responses of Shuey (1985) equation without ray bending for angles from 0° to 30° with a 1° increment.

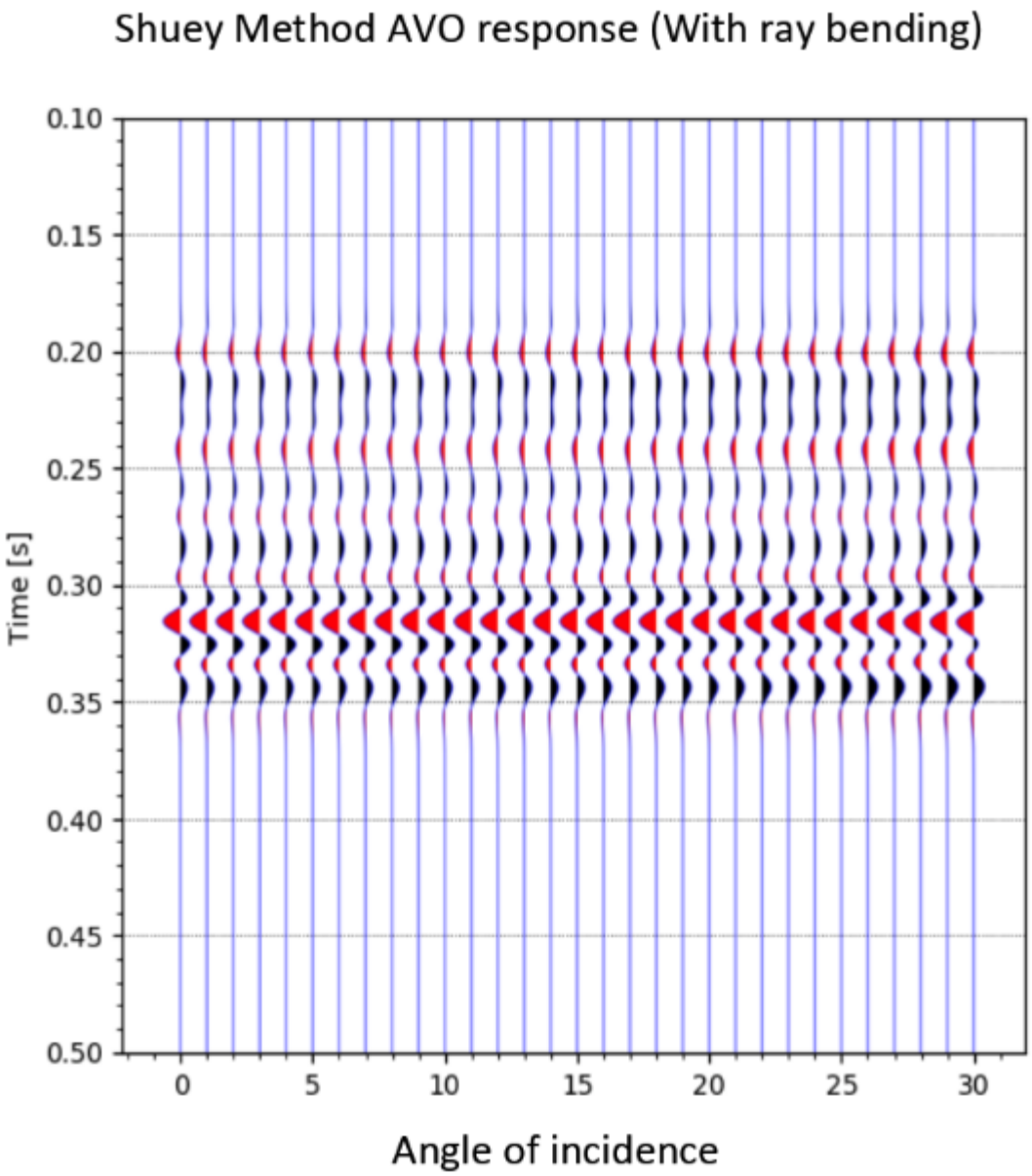

Figure 3.26. Synthetic data that shows responses of Shuey (1985) equation with ray bending for angles from 0° to 30° with 1° increments.

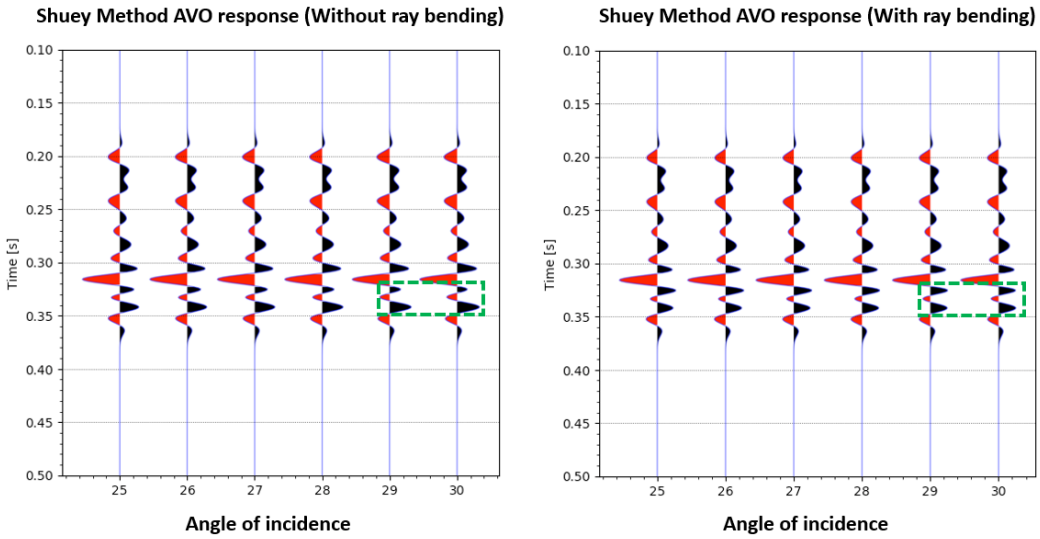

Figure 3.27. A closer look at the synthetic data responses of the Shuey (1985) equation with and without ray bending for angles from 25° to 30° with 1° increments.

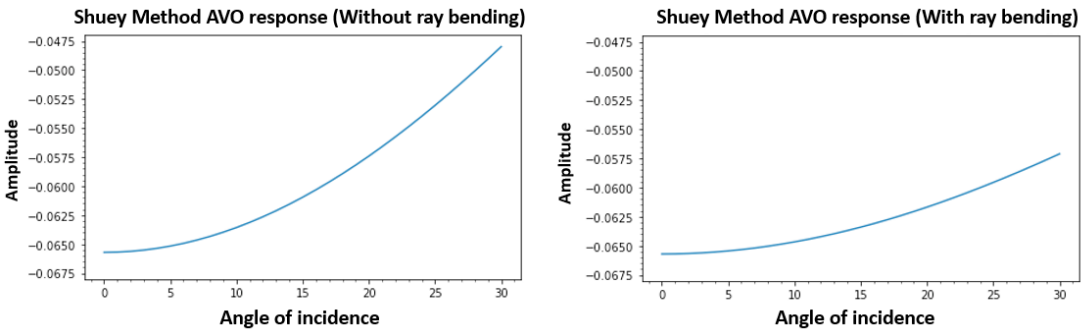

Figure 3.28. AVO response comparison between the Shuey (1985) equation without ray bending (on the left) and the Shuey (1985) equation with ray bending (on the right) for well log data.

3.5 AVO Analysis Comparison Between The Shuey Equation With and Without Ray Bending Vs. The Reflectivity Method

For my last test, I compared the results of the Shuey (1985) equation, with and without ray bending, vs. the Reflectivity Method. I used 200 layers from the well log data transition zone and compared the near and far offsets for all methods. My codes produced the responses in figures (3.29 - 3.31) for zero offset and figures (3.32 - 3.34) for the far offset.

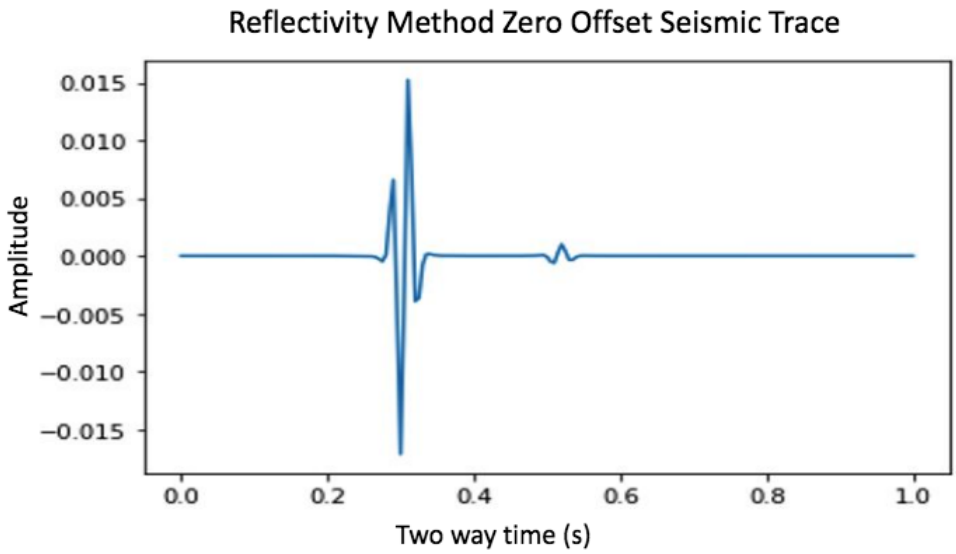

Figure 3.29. Zero offset seismic response of applying the Reflectivity Method on the well log data transition zone. Notice the presence of a low amplitude multiple.

The near offset plots show very similar waveform shapes. The Shuey (1985) equation plots, with and without ray bending, show similar amplitudes while the Reflectivity Method shows lower amplitude values. A low amplitude multiple can also be seen in the Reflectivity Method plot. The far offset plots also show good waveform shape similarities. However, the amplitudes of the Reflectivity Method are much smaller compared to the Shuey (1985) equation, with and without ray

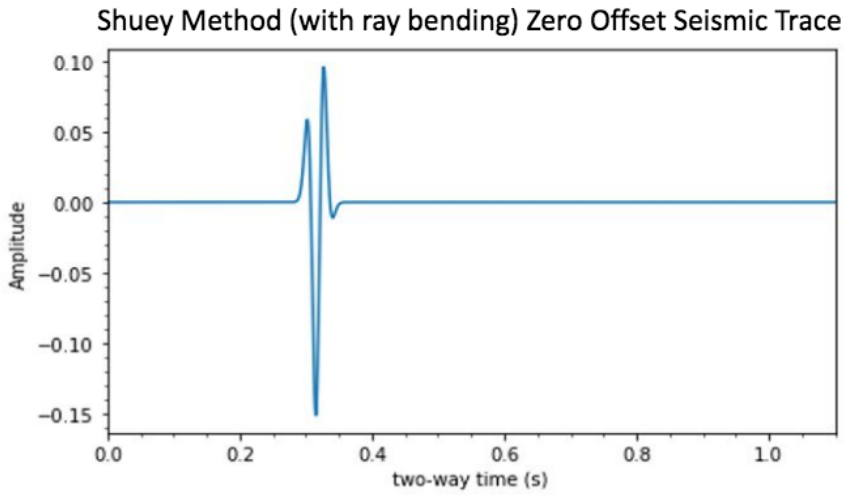

Figure 3.30. Zero offset seismic response of applying the Shuey (1985) equation with ray bending on the well log data transition zone. Notice the absence of multiples.

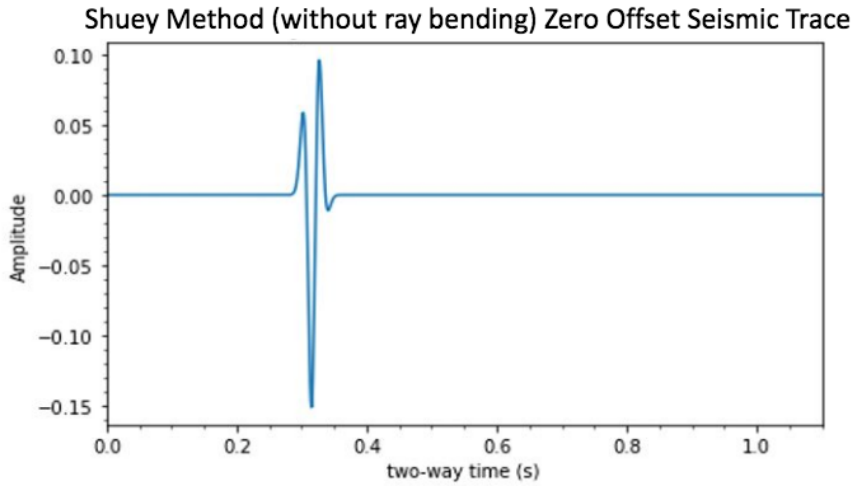

Figure 3.31. Zero offset seismic response of applying the Shuey (1985) equation without ray bending on the well log data transition zone. Notice the absence of multiples.

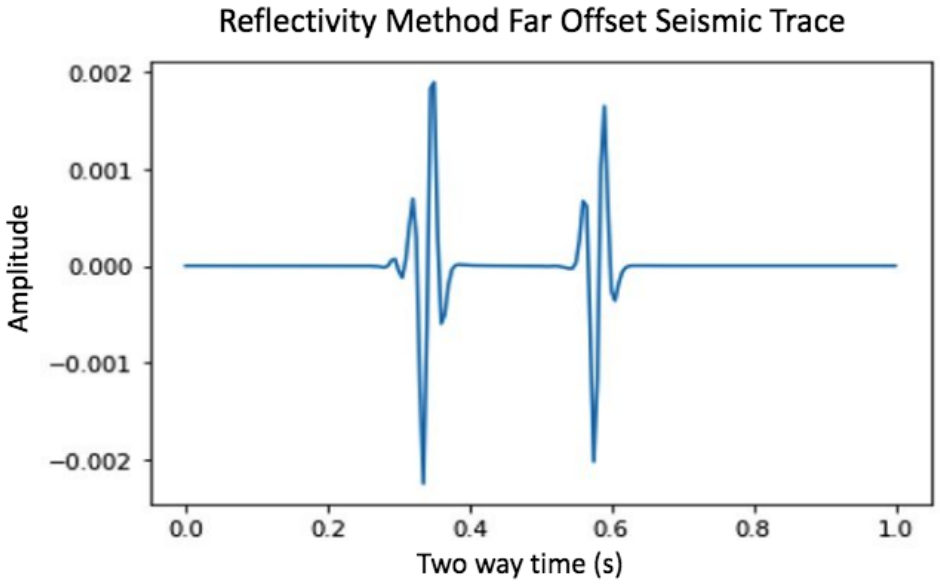

Figure 3.32. Far offset seismic response of applying the Reflectivity Method on the well log data transition zone. Notice the presence of a high amplitude multiple.

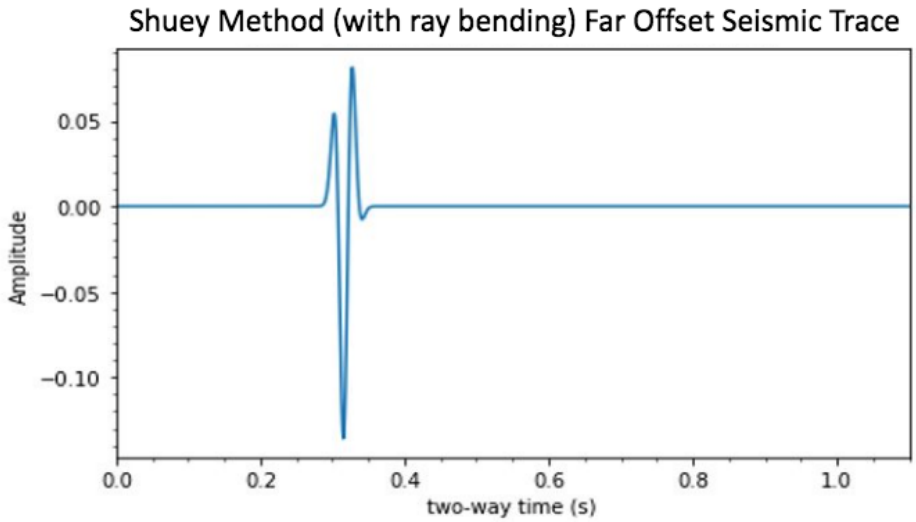

Figure 3.33. Far offset seismic response of applying the Shuey (1985) equation with ray bending on the well log data transition zone. Notice the absence of multiples.

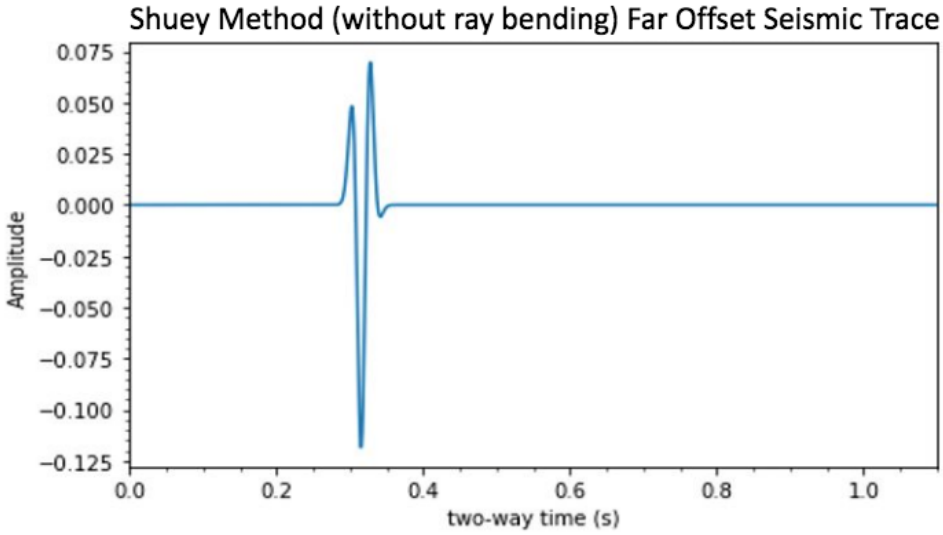

Figure 3.34. Far offset seismic response of applying the Shuey (1985) equation without ray bending on the well log data transition zone. Notice the absence of multiples.

bending due to the inclusion of multiples in the Reflectivity Method. A more pronounced higher amplitude multiple can also be seen in the Reflectivity Method plot.

Although the Reflectivity Method shows the correct seismic responses, it is limited by a long computational time. In contrast, the Shuey (1985) equation with ray bending shows acceptable responses with some degree of error. However, it has a short computational time. This advantage makes the Shuey (1985) equation with ray bending a good candidate to be applied in AVO analysis and seismic interpretation.

Chapter 4

Discussion

The main focus of my thesis was to investigate the effect of varying velocities and densities on thin layer characterization using tuning curves and AVO analysis. Then, evaluate the results when compared to equations which implement abrupt changes in velocities and densities (Velocity Block Models).

4.1 Assumptions and Limitations

As with any seismic test, initial assumptions concerning seismic data and models are made. The main assumption is the use of an idealized model where the Earth's subsurface is assumed to be composed of horizontal isotropic layers with constant velocities. However, in reality this is an unrealistic model. The subsurface is not ideally layered as one would assume for seismic interpretation. There are geological structure complexities, varying layer thicknesses and varying velocities. Because of this assumption the output of the seismic data will have some differences from the resulting model. Since the idealized model is isotropic, it does not account for anisotropic changes where velocity is affected by direction and

angle. If anisotropy was present, the velocity and amplitude of the the Primary Pulse Method equations will change as a function of direction and angle. However, I still believe the amplitude will go to infinity as thickness goes to zero.

4.2 Computational Time

One of the major concerns of seismic analysis is computational time. Some processes might take seconds while others take days to compute. In Richards and Frasier (1976) they used a transition zone model that consists of 67 or 53 layers. Calculating the Primary Pulse Method results was very quick (few minutes). Even when I Increased the number of layers to a 1000 layers that did not significantly impact computational time. Neither did increasing the number of iterations in the Trapezoidal Rule to 300. It also only took a few minutes to compute the results of applying the RPP equation and the Shuey equation (with and without ray bending) on well log data. Because of the fast computational time of the Primary Pulse Method, it could be suitable for inversion where a huge number of models are computed.

On the other hand, the Reflectively Method is limited by long computational times. However, this limitation is significant or negligible depending on its application. For the purposes of my thesis, I was testing simple models with different numbers of layers and thicknesses. Computing the result of a 200 layer model only took about 2 hours to finish. Hence, the Reflectivity Method in my case was appropriate. However, in the case of inversion for example, where a huge number of models are used, the reflectivity method would not be suitable.

4.3 Applications, Future work and Beyond

The Primary Pulse Method is flawed theoretically in the presence of thin layers but that might not be the case practically. In seismic analysis, the type of seismic data , the area of acquisition, the processing flow and data quality all contribute to seismic interpretation results. The method gave unrealistic results in the presence of thin layers when tested on the well log data I used. Nevertheless, that does not eliminate the possibility of its effectiveness on different models and scenarios. Future work could concentrate on the application of the Primary Pulse Method on a wider range of real seismic data models.

Since velocity is sensitive to tuning and in the presence of hydrocarbons, tuning curves can help in monitoring CO_2 injection in the presence of thin layers. Although a number of authors and publications (Chadwick *et al.* (2010), Furre *et al.* (2017), Romdhane *et al.* (2014), Velis and Rubino (2011), Williams and Chadwick (2012)) discussed different methods (Spectral Decomposition, Spectral Inversion and Full Waveform Inversion) for identifying CO_2 in the presence of thin layers, these methods assumed a velocity block model in their calculations. For that reason, the Primary Pulse Method, which assumes changes in velocity, might show potential in the detection of CO_2 in thin layers.

In my thesis, I discussed the effect of ray bending on seismic data where integrating it with the Shuey (1985) equation showed good potential in AVO analysis. Since this method has the advantage of fast computational times, it could be applied for inversion modeling. It might also have value in oil and gas exploration. Furthermore, it stands to reason that applying ray bending on current thin layer detection methods might have an impact on AVO analysis. The application of ray bending on these methods could produce different AVO response, which might lead to better identification of rock lithology and different gas-sand classes.

Chapter 5

Conclusion

The aim of my thesis was to investigate the effect of varying velocity and density on thin layer characterization using tuning curves and AVO analysis. Previous studies and publications concentrated on models with sudden changes in velocity (Velocity Block Model). However, in reality velocity varies in the layers of the subsurface. I identified Richards and Frasier (1976) Primary Pulse Method as a good candidate to study the effects of varying velocity.

In this thesis, I studied the seismic responses of the Primary Pulse Method when applied on thin layer models. This method takes into account gradual changes in velocity and density as the wave moves through a transition zone in contrast to sudden changes in velocity and density as with previously well-known methods (e.g. Shuey (1985)).

The Primary Pulse Method considers six primary reflection coefficient equations. I coded the equations and validated my results by comparing them to Richards and Frasier (1976) published results which showed good agreement.

Richards and Frasier (1976) was limited to the discussion of primary reflection coefficient equation responses. However, I sought to evaluate the seismic waveforms of the Primary Pulse Method. For my study, I convolved the primary reflection coefficient equation representing an incident P-wave reflected to the surface as a P-wave (RPP) with a Ricker wavelet. I chose the RPP equation since most seismic interpretation and analysis is done on primary waves.

The RPP convolution showed different waveform shapes than a Ricker wavelet. To further understand this outcome, I compared the RPP equation with the well-known reflection coefficient equation of Acoustic Impedance that takes into account sudden changes in velocity and density while also ignoring multiples.

The RPP convolution results showed different waveform shapes when compared to Acoustic Impedance. After investigating, I discovered that the RPP response waveform is an integration of the Ricker wavelet.

Richards and Frasier (1976) applied the Primary Pulse Method on a thick transition zone, usually seen for large scale earthquake models, where my interest was implementing the method for thin layer cases. The integrated wavelet response of the RPP is expected to have implications on thin layer tuning when the top and bottom responses interfere with each other as thickness goes to zero.

For my testing, I applied the RPP equation and Acoustic Impedance on different layered models to generate tuning curves. I noticed that the RPP amplitude responses increase to infinity as thickness goes to zero; which is unreasonable. In contrast, the Acoustic Impedance amplitudes go to zero as thickness goes to zero. I hypothesized that this infinite increase in amplitude might be a consequence of ignoring multiples.

To investigate the effect of ignoring multiples in the Primary Pulse Method, I compared the results of the RPP equation with the Reflectivity Method;

which takes into account multiples in its calculations but is limited by a long computational time. I compared the signal responses of both methods on a thick transition zone which showed that both methods have similar waveform shapes. I then plotted tuning curves for both methods to examine the responses in the presence of thin layers. The Reflectivity Method amplitudes go to zero as thickness goes to zero in contrast to the infinite amplitude increase in the RPP response. This confirmed my belief that the unrealistic amplitudes of the Primary Pulse Method in thin layer cases are a consequence of ignoring multiples.

Although the theory of the Primary Pulse Method is flawed in the presence of thin layers due to ignoring multiples, I sought to apply the method on well log data to investigate if this limitation would impact real seismic data. I applied the RPP equation and the Shuey (1985) equation on well log data to compare their seismic responses. The RPP equation responses still showed unrealistic high amplitudes. This confirms that the Primary Pulse Method also fails for real seismic data in the presence of thin layers.

One of the advantages of the Primary Pulse Method is considering the effect of ray bending which I sought to evaluate on AVO analysis.

For a fair comparison of the ray bending effect, I compared the AVO responses of the Shuey (1985) equation with and without ray bending for angles from 0° to 30°. Ray bending produced a more subtle and gradual increase in amplitude as angle of incidence increased, in contrast to a faster increase in amplitude when ignoring the ray bending effect. A point to note here is that the Shuey (1985) equation, with and without ray bending, has the advantage of a fast computational time.

Finally, I compared the AVO responses of the Reflectivity Method against the Shuey (1985) equation, with and without ray bending, on the well log data transition zone. Results showed similar waveform shapes at the near offset but

with lower amplitude values and a low amplitude multiple in the Reflectivity Method response. As for the far offset, the Reflectivity Method showed much smaller amplitude values than the Shuey (1985) plots, with and without ray bending and a high amplitude multiple in the Reflectivity Method response.

In conclusion, the Primary Pulse Method fails in the presence of thin layer cases theoretically and practically due to ignoring multiples. Second, even though the Reflectivity Method generates accurate AVO responses; since it includes multiples in its calculations, the method is limited by a long computational time. Because of this limitation, one might decide to use another faster method for AVO analysis and seismic interpretation. The Shuey (1985) equation with ray bending produced acceptable AVO responses which are less accurate when compared to the Reflectivity Method. However, the Shuey (1985) equation with ray bending has the advantage of a significantly faster computational time. Hence, it could be a good candidate for AVO analysis and seismic interpretation.

References

Abramowitz, M. and Stegun, I.A. (1965). *Handbook of mathematical functions: with formulas, graphs, and mathematical tables*, vol. 55. Courier Corporation.

Aki, K. and Richards, P. (1980). Quantitative seismology, theory and methods, vol. 1 wh freeman & co. *New York*.

Alnes, H., Eiken, O. and Stenvold, T. (2008). Monitoring gas production and co 2 injection at the sleipner field using time-lapse gravimetry. *Geophysics*, **73**, WA155–WA161.

Arts, R., Chadwick, A., Eiken, O., Thibeau, S. and Nooner, S. (2008). Ten years' experience of monitoring co2 injection in the utsira sand at sleipner, offshore norway. *First break*, **26**.

Atkinson, K.E. (2008). *An introduction to numerical analysis*. John Wiley & Sons.

Bakke, N. and Ursin, B. (1998). Thin-bed avo effects. *Geophysical Prospecting*, **46**, 571–587.

Ball, V. (1988). Thin bed tuning analysis using avo stratigraphy methods. In *SEG Technical Program Expanded Abstracts 1988*, 1213–1216, Society of Exploration Geophysicists.

Barclay, F., Bruun, A., Rasmussen, K.B., Alfaro, J.C., Cooke, A., Cooke, D., Salter, D., Godfrey, R., Lowden, D., McHugo, S. *et al.* (2008). Seismic inversion: Reading between the lines. *Oilfield Review*, **20**, 42–63.

Blangy, J. (1994). Avo in transversely isotropic mediaan overview. *Geophysics*, **59**, 775–781.

Boait, F., White, N., Bickle, M., Chadwick, R., Neufeld, J. and Huppert, H. (2012). Spatial and temporal evolution of injected co2 at the sleipner field, north sea. *Journal of Geophysical Research: Solid Earth*, **117**.

Bortfeld, R. (1961). Approximations to the reflection and transmission coefficients of plane longitudinal and transverse waves. *Geophysical Prospecting*, **9**, 485–502.

Braile, L.W. and Smith, R.B. (1975). Guide to the interpretation of crustal refraction profiles. *Geophysical Journal International*, **40**, 145–176.

Cambois, G. (1998). Avo attributes and noise: pitfalls of crossplotting. In *SEG Technical Program Expanded Abstracts 1998*, 244–247, Society of Exploration Geophysicists.

Carcione, J.M. and Tinivella, U. (2000). Bottom-simulating reflectors: Seismic velocities and avo effects. *Geophysics*, **65**, 54–67.

Castagna, J.P. and Backus, M.M. (1993). *Offset-dependent reflectivityTheory and practice of AVO analysis*. Society of Exploration Geophysicists.

Castagna, J.P. and Swan, H.W. (1997). Principles of avo crossplotting. *The leading edge*, **16**, 337–344.

Castagna, J.P., Batzle, M.L. and Eastwood, R.L. (1985). Relationships between compressional-wave and shear-wave velocities in clastic silicate rocks. *Geophysics*, **50**, 571–581.

Castagna, J.P., Swan, H.W. and Foster, D.J. (1998). Framework for avo gradient and intercept interpretation. *Geophysics*, **63**, 948–956.

Castaño, K.P. and Ojeda, G. (2010). Optimizing thin-layer mapping through spectral inversion: performance of genetic algorithms and simulated annealing. In *SEG Technical Program Expanded Abstracts 2010*, 1610–1614, Society of Exploration Geophysicists.

Castaño, K.P., Ojeda, G. and Montes, L. (2011). Thin-layer detection using spectral inversion and a genetic algorithm. *Earth Sciences Research Journal*, **15**, 121–128.

Chadwick, A., Williams, G., Delepine, N., Clochard, V., Labat, K., Sturton, S., Buddensiek, M.L., Dillen, M., Nickel, M., Lima, A.L. *et al.* (2010). Quantitative analysis of time-lapse seismic monitoring data at the sleipner co 2 storage operation. *The Leading Edge*, **29**, 170–177.

Chapman, C. (2003). Yet another elastic plane-wave, layer-matrix algorithm. *Geophysical Journal International*, **154**, 212–223.

Chiburis, E.F. (1984). Analysis of amplitude versus offset to detect gas/oil contacts in the arabian gulf. In *SEG Technical Program Expanded Abstracts 1984*, 669–670, Society of Exploration Geophysicists.

Chopra, S., Castagna, J. and Portniaguine, O. (2006). Seismic resolution and thin-bed reflectivity inversion: Canadian society of exploration geophysicists recorder. *Canadian Society of Exploration Geophysicists Recorder*.

Chung, H.M. and Lawton, D. (1999). A quantitative study of the effects of tuning on avo effects for thin beds. *Canadian Journal of Exploration Geophysics*, **35**, 36–42.

Chung, H.M. and Lawton, D.C. (1995). Amplitude responses of thin beds: Sinusoidal approximation versus ricker approximation. *Geophysics*, **60**, 223–230.

Dong, W. (1996). Fluid line distortion due to migration stretch. In *SEG Technical Program Expanded Abstracts 1996*, 1345–1348, Society of Exploration Geophysicists.

Dragoset, B. (2005). A historical reflection on reflections. *The Leading Edge*, **24**, S46–S71.

Farfour, M., Ferahtia, J., Djarfour, N. and Aitouch, M.A. (2017). 6. seismic spectral decomposition applications in seismic: A review and application. *Oil and Gas Exploration: Methods and Application*, **72**, 93.

Fatti, J.L., Smith, G.C., Vail, P.J., Strauss, P.J. and Levitt, P.R. (1994). Detection of gas in sandstone reservoirs using avo analysis: A 3-d seismic case history using the geostack technique. *Geophysics*, **59**, 1362–1376.

Foster, D. and Keys, R. (1999). Interpreting avo responses. In *SEG Technical Program Expanded Abstracts 1999*, 748–751, Society of Exploration Geophysicists.

Foster, D., Keys, R. and Reilly, J. (1997). Another perspective on avo crossplotting. *The Leading Edge*, **16**, 1233–1239.

Foster, D.J., Keys, R.G. and Lane, F.D. (2010). Interpretation of avo anomalies. *Geophysics*, **75**, 75A3–75A13.

Frasier, C.W. (1970). Discrete time solution of plane p-sv waves in a plane layered medium. *Geophysics*, **35**, 197–219.

Fryer, G.J. (1980). A slowness approach to the reflectivity method of seismogram synthesis. *Geophysical Journal International*, **63**, 747–758.

Fuchs, K. and Müller, G. (1971). Computation of synthetic seismograms with the reflectivity method and comparison with observations. *Geophysical Journal International*, **23**, 417–433.

Furre, A.K., Eiken, O., Alnes, H., Vevatne, J.N. and Kiær, A.F. (2017). 20 years of monitoring co2-injection at sleipner. *Energy procedia*, **114**, 3916–3926.

Gao, D. (2003). Volume texture extraction for 3d seismic visualization and interpretation. *Geophysics*, **68**, 1294–1302.

Garotta, R.J. and Grange, P.Y. (1987). Comparison of responses of compressional and converted waves on a gas sand. In *SEG Technical Program Expanded Abstracts 1987*, 627–630, Society of Exploration Geophysicists.

Goodway, B., Chen, T. and Downton, J. (1997). Improved avo fluid detection and lithology discrimination using lamé petrophysical parameters;$\lambda\rho$,$\mu\rho$, & λ/μ fluid stack, from p and s inversions. In *SEG Technical Program Expanded Abstracts 1997*, 183–186, Society of Exploration Geophysicists.

Granli, J.R., Arntsen, B., Sollid, A. and Hilde, E. (1999). Imaging through gas-filled sediments using marine shear-wave data. *Geophysics*, **64**, 668–677.

Gray, D., Goodway, B. and Chen, T. (1999). Bridging the gap: Using avo to detect changes in fundamental elastic constants. In *SEG Technical Program Expanded Abstracts 1999*, 852–855, Society of Exploration Geophysicists.

Haskell, N.A. (1953). The dispersion of surface waves on multilayered media. *Bulletin of the seismological Society of America*, **43**, 17–34.

Hesthammer, J., Landrø, M. and Fossen, H. (2001). Use and abuse of seismic data in reservoir characterisation. *Marine and Petroleum Geology*, **18**, 635–655.

Hilterman, F. (1990). Is avo the seismic signature of lithology? a case history of ship shoal-south addition. *The Leading Edge*, **9**, 15–22.

Hilterman, F.J. (1989). Is avo the seismic signature of rock properties? In *SEG Technical Program Expanded Abstracts 1989*, 559–559, Society of Exploration Geophysicists.

Hindlet, F.J. and McDonald, J.A. (1986). Thin layer analysis using off-set/amplitude data. In *SEG Technical Program Expanded Abstracts 1986*, 346–349, Society of Exploration Geophysicists.

Huang, Z.l. and Zhang, J. (2013). A step-by-step algorithm for spectral inversion. In *SEG Technical Program Expanded Abstracts 2013*, 4699–4703, Society of Exploration Geophysicists.

James, H. (2003). Has volume interpretation of structure been cracked at last? *First Break*, **21**.

James, H. (2009). Visualizing 3d features in 3d seismic data. *First Break*, **27**.

Kamei, R. and Lumley, D. (2015). Estimating time-lapse velocity changes in the earth by full waveform inversion of repeating seismic events. In *AGU Fall Meeting Abstracts*.

Kelly, M.C. and Ford, D. (2000a). The interpretation of pp avo cross-plots. In *SEG Technical Program Expanded Abstracts 2000*, 214–217, Society of Exploration Geophysicists.

Kelly, M.C. and Ford, D. (2000b). Ps avo attributes and cross-plotting. In *SEG Technical Program Expanded Abstracts 2000*, 218–221, Society of Exploration Geophysicists.

Kempner, W. and Gettrust, J. (1982a). Ophiolites, synthetic seismograms, and ocean crustal structure: 1. comparison of ocean bottom seismometer data and synthetic seismograms for the bay of islands ophiolite. *Journal of Geophysical Research: Solid Earth*, **87**, 8447–8462.

Kempner, W.C. and Gettrust, J.F. (1982b). Ophiolites, synthetic seismograms, and oceanic crustal structure: 2. a comparison of synthetic seismograms of the samail ophiolite, oman, and the rose refraction data from the east pacific rise. *Journal of Geophysical Research: Solid Earth*, **87**, 8463–8476.

Kennett, B. (1975). The effects of attenuation on seismograms. *Bulletin of the Seismological Society of America*, **65**, 1643–1651.

Kennett, B. (1979). Theoretical reflection seismograms for elastic media. *Geophysical Prospecting*, **27**, 301–321.

Kennett, B. (1980). Seismic waves in a stratified half spaceii. theoretical seismograms. *Geophysical Journal International*, **61**, 1–10.

Kennett, B. and Clarke, T. (1983). Seismic waves in a stratified half-spaceiv: Psv wave decoupling and surface wave dispersion. *Geophysical Journal International*, **72**, 633–645.

Kennett, B. and Illingworth, M. (1981). Seismic waves in a stratified half spaceiii. piecewise smooth models. *Geophysical Journal International*, **66**, 633–675.

Kind, R. (1976). Computation of reflection coefficients for layered media. *JOURNAL OF GEOPHYSICS-ZEITSCHRIFT FUR GEOPHYSIK*, **42**, 191–200.

Knott, C.G. (1899). Iii. reflexion and refraction of elastic waves, with seismological applications. *The London, Edinburgh, and Dublin Philosophical Magazine and Journal of Science*, **48**, 64–97.

Loizou, N., Liu, E. and Chapman, M. (2008). Avo analyses and spectral decomposition of seismic data from four wells west of shetland, uk. *Petroleum Geoscience*, **14**, 355–368.

Mahmoudian, F. and Margrave, G.F. (2007). P-wave impedance, s-wave impedance and density from linear avo inversion: Application to vsp data from alberta. In *CSPG CSEG convention*.

Mallick, S. and Frazer, L.N. (1987). Practical aspects of reflectivity modeling. *Geophysics*, **52**, 1355–1364.

Milligan, M. (2004). What are seismic surveys and how much shaking do they create. *Utah Geological Survey Notes*, **36**, 10–11.

Mondol, N.H. (2010). Seismic exploration. In *Petroleum Geoscience*, 375–402, Springer.

O'neill, M. and Hill, D.P. (1979). Causal absorption: Its effect on synthetic seismograms computed by the reflectivity method. *Bulletin of the Seismological Society of America*, **69**, 17–25.

Ongkiehong, L. and Askin, H. (1988). Towards the universal seismic acquisition technique. *First Break*, **6**, 46–63.

Papageorgiou, G. and Ivanov, Y. (2018-2019). Codes for the project "interpretation of frequency-dependent seismic responses of finely layered, partially saturated and fractured reservoirs". https://github.com/yuriyi/PM2-codes.

Papoulis, A. (1962). *The Fourier Integral and Its Applications. Papoulis*. McGraw-Hill.

Ratcliffe, A., Win, C., Vinje, V., Conroy, G., Warner, M., Umpleby, A., Stekl, I., Nangoo, T. and Bertrand, A. (2011). Full waveform inversion: A north sea obc case study. In *SEG Technical Program Expanded Abstracts 2011*, 2384–2388, Society of Exploration Geophysicists.

Richards, P.G. and Frasier, C.W. (1976). Scattering of elastic waves from depth-dependent inhomogeneities. *Geophysics*, **41**, 441–458.

Romdhane, A., Querendez, E. and Ravaut, C. (2014). Co2 thin-layer detection at the sleipner field with full waveform inversion: Application to synthetic and real data. *Energy procedia*, **51**, 281–288.

Rutherford, S.R. and Williams, R.H. (1989). Amplitude-versus-offset variations in gas sands. *Geophysics*, **54**, 680–688.

Schmid, L., Schweizer, J., Bradford, J. and Maurer, H. (2016). A synthetic study to assess the applicability of full-waveform inversion to infer snow stratigraphy from upward-looking ground-penetrating radar data. *Geophysics*, **81**, WA213–WA223.

Selley, R.C. and Sonnenberg, S.A. (2014). *Elements of petroleum geology*. Academic Press.

Sheriff, R. (1976). Inferring stratigraphy from seismic data. *AAPG Bulletin*, **60**, 528–542.

Sheriff, R.E. and Geldart, L.P. (1995). *Exploration seismology*. Cambridge university press.

Shuey, R. (1985). A simplification of the zoeppritz equations. *Geophysics*, **50**, 609–614.

Simm, R. (2009). Simple net pay estimation from seismic: A modelling study. *first break*, **27**, 45–53.

Sipkin, S., Orcutt, J. and Jordan, T. (1978). Examination of scs travel times with a causal q reflectivity algorithm for sh polarized waves. *TRANSACTIONS-AMERICAN GEOPHYSICAL UNION*, **59**, 324–324.

Smith, G. and Gidlow, P. (1987). Weighted stacking for rock property estimation and detection of gas. *Geophysical Prospecting*, **35**, 993–1014.

Spudich, P. and Orcutt, J. (1980a). A new look at the seismic velocity structure of the oceanic crust. *Reviews of Geophysics*, **18**, 627–645.

Spudich, P. and Orcutt, J. (1980b). Petrology and porosity of an oceanic crustal site: Results from wave form modeling of seismic refraction data. *Journal of Geophysical Research: Solid Earth*, **85**, 1409–1433.

Stephen, R. (1977). Synthetic seismograms for the case of the receiver within the reflectivity zone. *Geophysical Journal International*, **51**, 169–181.

Stovas, A. and Ursin, B. (2003). Reflection and transmission responses of layered transversely isotropic viscoelastic media. *Geophysical Prospecting*, **51**, 447–477.

Swan, H.W. (1988). Amplitude versus offset analysis in a finely layered media. In *SEG Technical Program Expanded Abstracts 1988*, 1195–1198, Society of Exploration Geophysicists.

Telford, W., Geldart, L., Sheriff, R. and Keys, D. (1976). Applied geophysics cambridge university press. *Cambridge*, **860**.

Thomson, W.T. (1950). Transmission of elastic waves through a stratified solid medium. *Journal of applied Physics*, **21**, 89–93.

Ursin, B. (1990). Offset-dependent geometrical spreading in a layered medium. *Geophysics*, **55**, 492–496.

Ursin, B. and Dahl, T. (1992). Seismic reflection amplitudes. *Geophysical Prospecting*, **40**, 483–512.

Ursin, B. and Ekren, B.O. (1995). Robust avo analysis. *Geophysics*, **60**, 317–326.

Velis, D.R. and Rubino, J.G. (2011). Quantitative characterization of co2-bearing thin layers at the sleipner field using spectral inversion. In *SEG Technical Program Expanded Abstracts 2011*, 2502–2506, Society of Exploration Geophysicists.

Ville, J. (1948). Theorie et application dela notion de signal analytique. *Câbles et transmissions*, **2**, 61–74.

Widess, M. (1973). How thin is a thin bed? *Geophysics*, **38**, 1176–1180.

Wigner, E.P. (1997). On the quantum correction for thermodynamic equilibrium. In *Part I: Physical Chemistry. Part II: Solid State Physics*, 110–120, Springer.

Williams, G. and Chadwick, A. (2012). Quantitative seismic analysis of a thin layer of co 2 in the sleipner injection plume. *Geophysics*, **77**, R245–R256.

Xie, Z. (2005). Application of 3d avo interpretation technique to lithological reservoir in the hongze area. *Applied Geophysics*, **2**, 168–174.

Yilmaz, Ö. (2001). *Seismic data analysis: Processing, inversion, and interpretation of seismic data*. Society of exploration geophysicists.

Zhang, H. and Brown, R. (2001). A review of avo analysis. *CREWES Res. Rep.*, **13**, 337–378.

Zoeppritz, K. (1919). On the reflection and propagation of seismic waves: Gottinger nachrichten, i, 66–84. *Google Scholar*.